Urban Forestry & Urban Greening 87 (2023) 128061

Contents lists available at ScienceDirect

Urban Forestry & Urban Greening

journal homepage: www.elsevier.com/locate/ufug

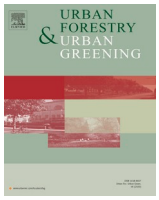

Spatio-temporal analysis of the urban green infrastructure of the city of Granada (Spain) as a heat mitigation measure using high-resolution images Sentinel 3

David Hidalgo García [*,1]

University of Granada. Technical Superior School of Building Engineering, University of Granada. Fuentenueva Campus, 18071 Granada, Spain

ARTICLE INFO

Keywords:
Land surface temperature
Sentinel 3
Park cool island
Urban green infrastructure
Urban heat mitigation

ABSTRACT

At present, and motivated by a substantial growth of the population, a considerable expansion of urban areas is taking place through the modification of land uses. These changes, together with global warming and extreme weather events, produce increases in the temperature of the earth's surface and a deterioration of the environment that affects people's quality of life. The green areas of cities are upheld as one of the best for adapting to such phenomena, since they help lower outdoor temperatures. In this research, using high-resolution Sentinel 3 satellite images and the TsHARP algorithm, the Land Surface Temperature (LST) and the Park Cool Island (PCI) were obtained at a resolution of 10 m over green areas in the city of Granada. The objective was to analyze the relationship between surface, PCI effect and cooling distance. In turn, for each of the eight green areas studied, the following variables were taken into account and included in a statistical analysis known as data panel: normalized difference vegetation index, vegetal proportion, sky view factor, landscape shape index, model digital elevation, wind and solar radiation. Our results report diurnal LST decreases of 1 K and night LST of 0.6 K in green areas as compared to urban areas. There is moreover a correlation between the size of the green areas, the decrease in temperature they generate, and distance of the minimizer effect.

1. Introduction

Currently, extreme weather events such as droughts, heat waves and floods linked to global climate change stand as an utmost challenge faced by humanity (An et al., 2020; Kovats et al., 2005; Song et al., 2020). The high growth of the population is a process that contributes to climate change through the transformation and modification of land, i.e. the expansion of urbanized areas (Li et al., 2011; Song et al., 2020). Recent estimates by the United Nations predict that by 2050 the urban population will increase by 20% (UN, 2018). The projection of a population increase of 2.5 billion people will possibly modify the global urban coverage by 1,600,000 km2 (Mukherjee and Debnath, 2020; Schneider et al., 2010). Although the expansion of industrial and urban areas and spaces for transport is the main driver of the economy, it alters the local urban climate through increases in the Land Surface Temperature (LST) (Hidalgo and Arco, 2021; Ray et al., 2020; Song et al., 2020). Numerous recent studies report higher LST values for urban areas as opposed to rural areas (Guo et al., 2020; Hidalgo and Arco, 2022; Hua et al., 2020; Karakuş, 2019). Not only do cities suffer the greatest increases in LST —they increase even more due to the Urban Heat Island (UHI) phenomenon and environmental pollution from the transport and industry sectors (Santamouris, 2020). Thus, a city with a population of approximately one million inhabitants may present an average temperature 1–3 K higher than rural areas (Khamchiangta and Dhakal, 2019). It is evident that the UHI, together with the increases in LST, can generate a series of economic, social, climatic and environmental problems that minimize the quality of life of people living in cities (Das and Das, 2020; Dwivedi and Mohan, 2018; Santamouris, 2020). Changes underway include the reduction of biodiversity, shifts in the energy balance, degradation of water and air quality, greater energy consumption, and even increased mortality (Arbuthnott and Hajat, 2017; Čeplová et al., 2017; Sarrat et al., 2006).

In recent years, the planning of green areas within new urban developments has acquired a fundamental role in territorial and political planning, since it allows the well-being of the population. In addition, it can be used as a tool to protect and promote the integrity and

* Corresponding author.
E-mail address: dhidalgo@ugr.es.
[1] ORCID: https://orcid.org/0000–0002-4039-8709

https://doi.org/10.1016/j.ufug.2023.128061
Received 8 November 2022; Received in revised form 18 July 2023; Accepted 8 August 2023
Available online 10 August 2023

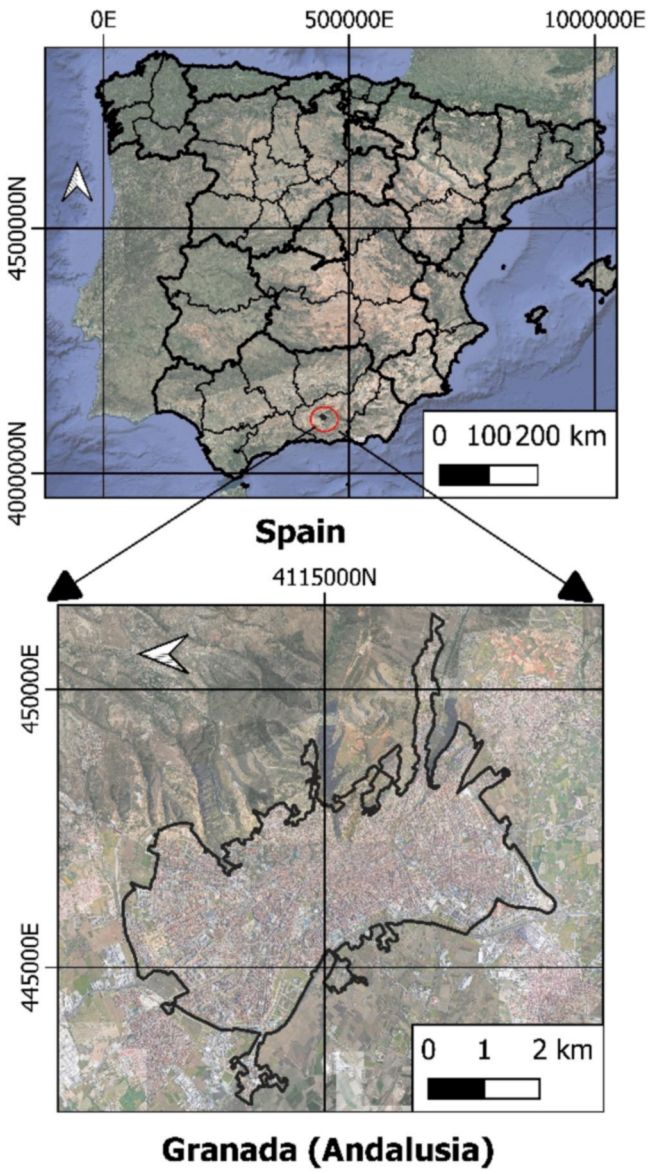

Fig. 1. Study Area: Granada, Andalusia, Spain.

sustainability of these areas. Therefore, any process of urban expansion requires planning the different spaces for all compatible uses: residential, green, industrial, etc. Usually, these works fall on the public administrations that have an adequate capacity to promote urban centers green, sustainable and healthy. The use of Urban Green Infrastructures (UGI) and the homogeneous distribution of trees in streets and open spaces in cities are considered effective strategies to mitigate urban heat and enhancing human comfort (Saaroni et al., 2018). They are included within the "microclimate transformation techniques" involving modifications of the physical environment through the use of vegetation (Gago et al., 2013; Norton et al., 2015; Saaroni et al., 2018; Solecki et al., 2005). New green spaces make it possible to reduce the LST and minimize the effects of the UHI, thus improving the quality of life of local inhabitants. The shade generated by the trees prevents solar radiation from heating up the impermeable walls, which therefore emit less heat into the atmosphere (Hidalgo and Arco, 2021). Meanwhile, the evapotranspiration of plant elements, allowing them to release part of their moisture into the atmosphere, has an environmental cooling effect and leads to a decrease in LST (Gago et al., 2013; Solecki et al., 2005).

The effect of temperature (in this research, LST) differences between urban areas and green areas is known as Park Cool Island (PCI) (Oliveira et al., 2011) and has been regularly studied. For example, a study on the city of Mumbai (India) in 2018 reported that the green areas of the city present differences with urban areas amounting to 2 or 3 K (Dwivedi and Mohan, 2018); the city of Singapore between the years 2005 and 2015 denoted a cooling effect of the green areas of 1–3 K (Masoudi et al., 2021); and the city of Shenzhen (China) reported a drop in temperature of 0.9–1.6 K between 2011 and 2013 (Qiu et al., 2017). Therefore, it is evident that green spaces have lower LST values than urban areas and should be studied for the purpose of mitigating high temperatures. It is vitally important, however, to know if this effect is related to the size or extension, morphology or coverage of green areas. Along these lines, a study on the city of Chongqing (China) reported that green areas with a minimum size of 35 m represented a reduction of the LST of between 1 and 1.5 K with respect to urban areas (Lu et al., 2012). A study of the city of Beijing (China) revealed that the cooling effects in large green areas extend up to 840 m in length from the edge of the area, but the effect in small green areas extends only up to 35 m (Lin et al., 2015). On the other hand, the study on 4 green spaces in the city of Wroclaw (Poland) reported a PCI of between 1 and 2 K and a cooling distance of between 110 and 925 m (Blachowski and Hajnrych, 2021). The study on the Retiro park in the city of Madrid (Spain) reported a cooling distance of between 130 and 280 m (Aram et al., 2020). Further research reports that large areas covered with trees are the ones that most reduce the LST during the day (Yoshida et al., 2015), while at night green lawn areas afford the greatest reduction in LST (Spronken-Smith, 2010).

Since the 1980 s, remote sensing has become commonly used to determine urban climate change phenomena. Satellite images obtained with thermal infrared sensors (TIRS) allow researchers to carry out urban studies of LST, Surface Urban Heat Island (SUHI) and PCI (Song et al., 2018). Satellites that have smaller pixel sizes such as Landsat (100–120 m) or ECOSTRESS (60 m) only orbit each point on the planet once a day, and always at the same time. Therefore, the results of these studies ultimately reflect the day or days chosen and the time of passage of the satellite, which is always the same. Notwithstanding, they extrapolate the results obtained in a timely manner to longer periods with the aim of deriving global results. Recent research (Anjos et al., 2020; Emmanuel and Krüger, 2012; Hidalgo and Arco, 2021) has reported that this is an erroneous operation, since there is a high variability of the LST, SUHI and PCI throughout the day. This circumstance highlights the need to work with satellites that orbit the same point on the earth's surface several times a day, such as Sentinel or Modis. In turn, these have a major drawback in that the pixel size of the thermal images is 1000 m, inadequate for the study of medium and small green areas. As a solution, it is possible to apply a Sharpening process to transform low resolution images (pixel size 1000 m) into new high resolution images (pixel size 10 m). Although there are numerous processes, the TsHARP algorithm stands out for its high precision and quality, used and verified in numerous studies (Belgiu and Stein, 2019; Huryna et al., 2019; Zhou et al., 2020). They have reported high values of precision and validity of this methodology. Accordingly, high-resolution Sentinel 3 images prove more accurate, giving correct results for the space-time variability of PCI in green areas.

The objective of this research is to analyze the space-time variability of the PCI on 8 green spaces of different sizes in the city of Granada (Spain) and determine what factors might influence the cooling distance. This is done through Sentinel 3 satellite images transformed to high resolution using the TsHARP algorithm. In addition to arriving at accurate figures for the LST and the PCI of the green areas, based on Sentinel 2 images, we determined the Normalized Difference Vegetation Index (NDVI), Vegetal Proportion (PV) and the Landscape Shape Index (LSI). Then, for each space, the Digital Elevation Model (DEM) obtained from the LIDAR data was taken into account and the variables of wind, solar radiation and Sky View Factor (SVF) could be modelled. The statistical techniques of Data Panel and ANOVA served to determine correlations between the variables.

In short, the questions we intend to answer through this study are: 1.

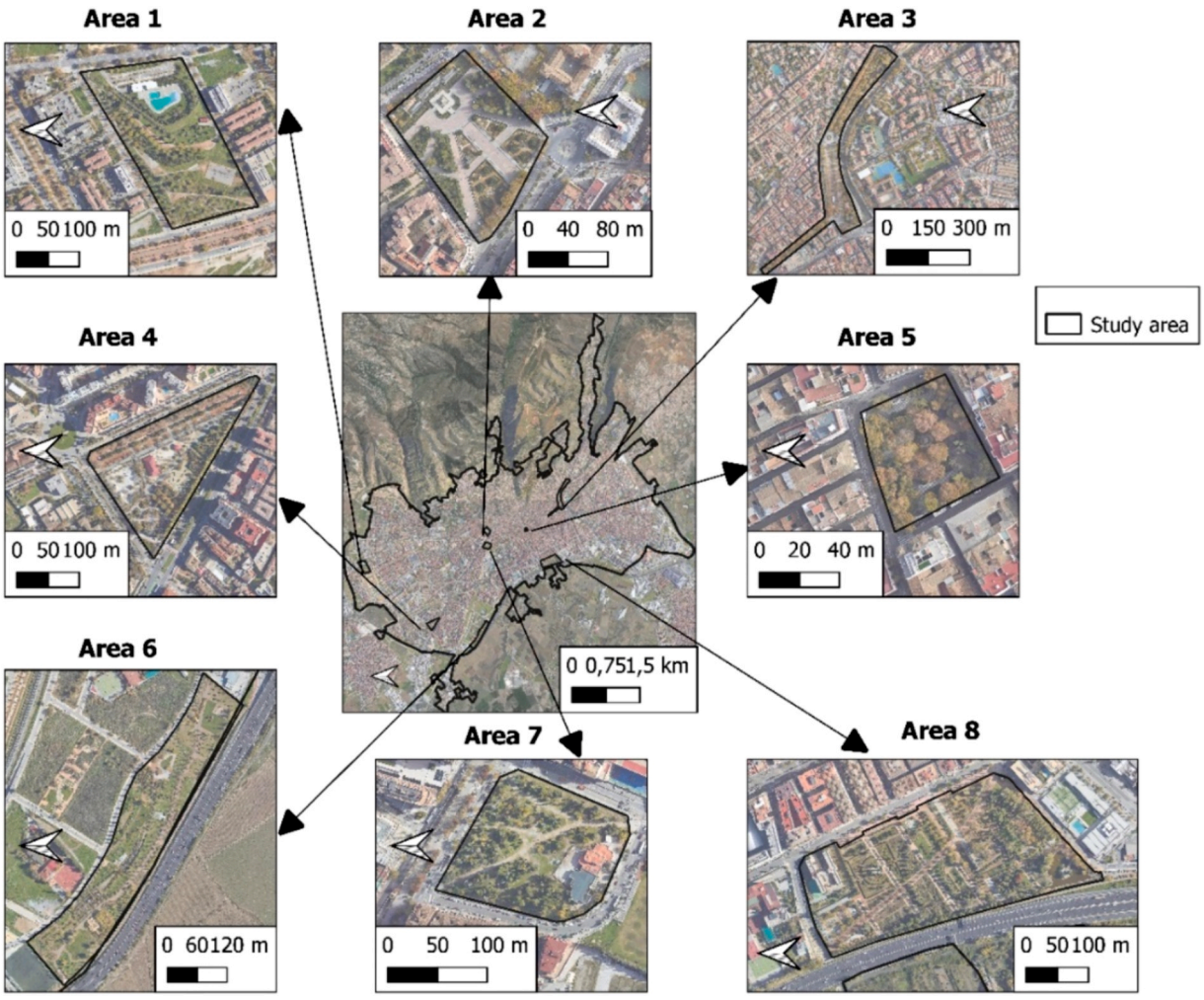

Fig. 2. Spaces selected for the study.

Table 1
Characteristics of city zones.

Area	Name	Area (m^2)	Maximum length (m)	DEM (m.a.s.l.)	LSI	Surface
1	Almanjayar	19363	218	708	1.2	Trees and albero
2	Triunfo	16234	128	685	1.1	Trees and pavement
3	Carrera de la Virgen	62836	561	670	2.5	Trees and albero
4	Almunia	32248	218	661	1.3	Trees and albero
5	Trinidad	3223	150	678	1.2	Trees and pavement
6	Alquerias	68594	388	643	1.7	Trees and grass
7	Fuentenueva	19216	135	675	1.1	Trees and grass
8	Federico García Lorca	76844	350	659	1.3	Trees and albero

Note: DEM: Digital Elevation Model; LSI: Landscape Shape Index

How does the space-time variability of LST and PCI develop in the green spaces studied in the city using high-resolution Sentinel 3 images? 2. What is the PCI attenuation distance, and what factors influence it? 3. Is there any relationship among the indices taken into account? 4. Can the results obtained be useful for future urban planning of green spaces?

The advances produced by this research help to glimpse the spatio-temporal variability of the PCI of the green areas of a medium-sized city (Granada) and the factors that modify it. There are numerous studies carried out on large cities, but few on small and medium-sized cities. These usually use LST images obtained from the Landsat satellite, which have a resolution of 120 m. Our research opens the door to the use of Sentinel by improving the resolution of the LST at 10 m and being able to improve the precision of the results. On the other hand, our study breaks with the tradition of using a single satellite image per year to analyze the evolution of the LST and other indices by using 10 daytime images and another 10 nighttime images. The ultimate aim is to promote more appropriate decision-making by urban planners and public administrations when developing new areas or green spaces. Decisions and actions should be directed at mitigating the effects of increases in LST and SUHI in cities, turning urban areas into environments that are resilient to climate change, so as to improve people's quality of life. The methodology applied here involved an open source QGIS work environment in order to be able to extrapolate the results obtained to other areas.

2. Materials and methods

2.1. Study area

The area under study (Fig. 1) consists of eight green spaces located in the city of Granada, within the region of Andalusia, southern Spain.

The UTM geographic coordinates of the city are: latitude 37.111741 N and longitude 03.362401 W; its altitude is 680 m above

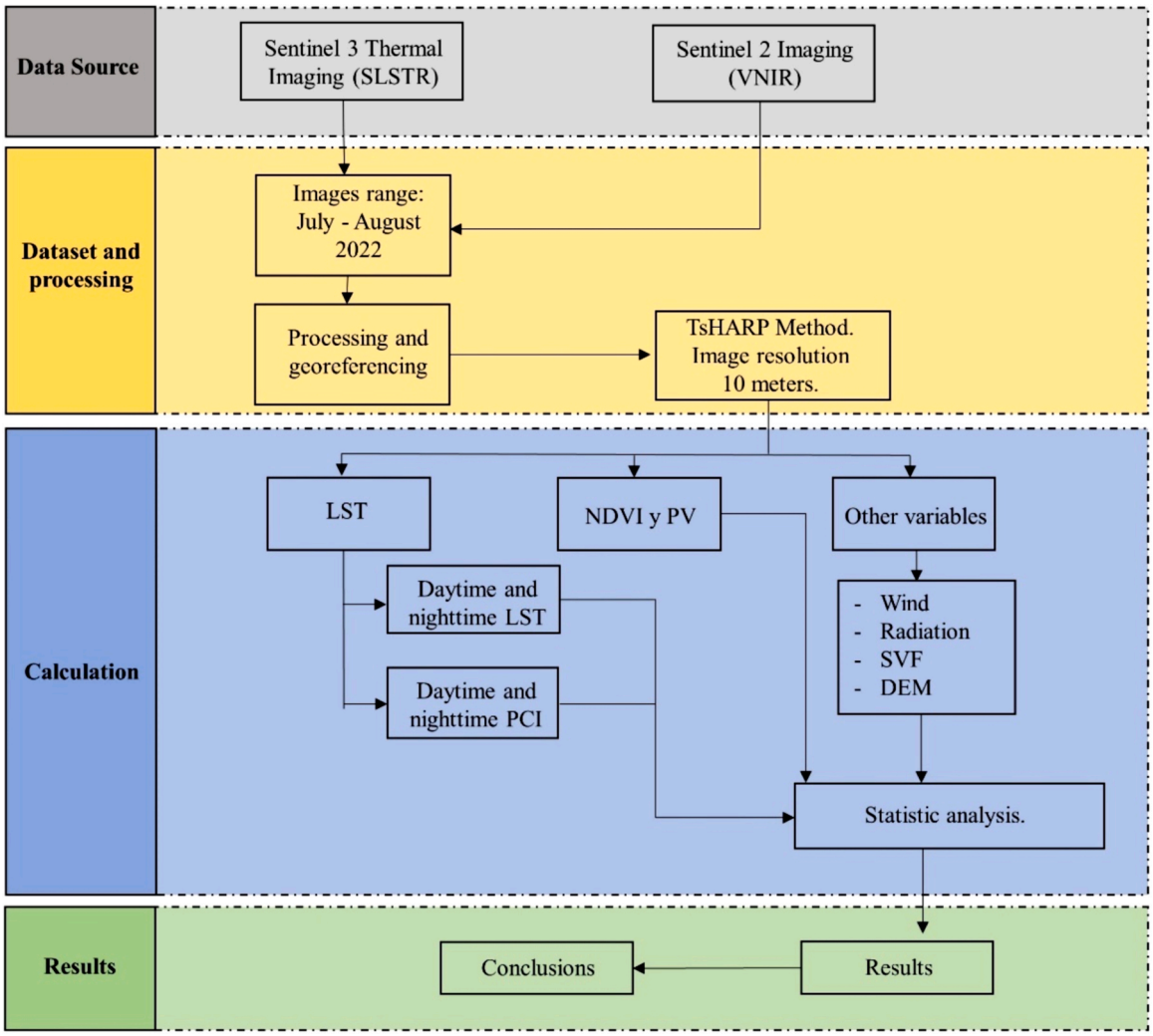

Fig. 3. Methodology.

sea level. This city has a population of 232,462 and occupies an area of 88 km^2. Its climate, according to the Köppen-Geiger classification, is of the Mediterranean type (Csa), which implies hot and dry summers and wet and cold winters (de Castro et al., 2007). The local climate is strongly conditioned by the proximity of the Sierra Nevada mountain range. It has an average altitude of 2045 m, reaching a maximum altitude of 3482 m at the Mulhacen peak. The average temperature fluctuates between 279.65 K in January and 298.45 K in July, with a winter minimum of 270.15 K and extremes in summer reaching 316.15 K. The approximate number of hours of sunshine per year is 2917, giving an average of 7.99 h of sunshine per day.

2.2. Data resources

The eight selected spaces are the largest green areas that are within the city limits and whose distribution is represented in Fig. 2. The surface, dimensions, coverage and morphology can be consulted in Table 1.

2.3. Methods

The methodology carried out is outlined in Fig. 3.

The NDVI and PV index of the areas under study were determined using Sentinel 2 images at a resolution of 10 m. Thermal images from Sea and Land Surface Temperature Radiometers (SLSTR) at a resolution of 1000 m, plus NDVI and PV images from the Ocean and Land Cover Instrument (OLCI) multispectral sensor at a resolution of 500 m, were downloaded. All images were obtained by means of the Copernicus Open Access Hub application and underwent band reclassification and atmospheric correction using the European Space Agency's (ESA) Sentinel Application Platform (SNAP) open source software. Then, taking the NDVI and PV images from Sentinel 2 and the TsHARP algorithm as a reference, the NDVI, PV and LST images from Sentinel 3 were resampled to a new resolution of 10 m. This procedure for obtaining high-resolution images is documented by the scientific community (Belgiu and Stein, 2019; Huryna et al., 2019) and presents excellent results. Afterwards, the PCI of the investigated green areas was determined using the raster calculator tool of QGIS 3.22.10 software. DEM and coverage data were obtained from the National Geographic Institute (IGN) of the Government of Spain at a resolution of 2.5 m. The SVF, wind and radiation variables were modelled for the same dates as the Sentinel 2 and 3 satellite images using SAGA 8.3.0 software, likewise supported by the scientific community as presenting good results (Conrad et al., 2015; Hidalgo and Arco, 2021; Olaya and Conrad, 2009). Finally, the statistical study of our research findings relied on specialized software for data science, STATA version 16.

2.4. Sentinel 2 images

The Sentinel 2 satellites make it possible to obtain high-resolution images of the earth's surface (10 m) thanks to the 12 bands having a

Table 2
Sentinel 2 A-B images used, acquired from the Copernicus Open Access Hub service.

Number	Date (yyyymmdd)	UTC time (hhmmss)	Cloudiness (%)
1	20220701	100512	5
2	20220704	103421	6
3	20220708	101304	2
4	20220712	100512	1
5	20220715	100921	5
6	20220721	101212	2
7	20220726	102305	0
8	20220809	105132	0
9	20220815	101201	4
10	20220828	103427	3
11	20220701	211612	2
12	20220704	221216	4
13	20220708	222354	2
14	20220712	221504	0
15	20220715	221832	5
16	20220721	215939	2
17	20220726	213912	2
18	20220709	215448	0
19	20220815	220508	4
20	20220828	221031	4

Table 3
Sentinel 3 A-B images used, acquired from the Copernicus Open Access Hub service.

Number	Date (yyyymmdd)	UTC time (hhmmss)	Cloudiness (%)
1	20220701	102921	5
2	20220704	105112	6
3	20220708	104805	2
4	20220712	104421	1
5	20220715	100429	5
6	20220721	104129	2
7	20220726	101955	0
8	20220809	105728	0
9	20220815	100815	4
10	20220828	102540	3
11	20220701	214616	2
12	20220704	220843	4
13	20220708	220512	2
14	20220712	220116	0
15	20220715	222343	5
16	20220721	212737	2
17	20220726	213650	2
18	20220709	213504	0
19	20220815	221958	4
20	20220828	220845	4

resolution that ranges between 10 and 60 m. The earth's surface and its changes can thus be monitored accurately through high-resolution images. In this case, 10 daytime images and another 10 nighttime images, distributed evenly between the months of July and August of the year 2022, were selected (Table 2). All of them have a cloudiness index of less than 5%. The images were obtained through the ESA Copernicus Open Access Hub with a level of detail type 2. After downloading the images, they were atmospherically corrected and georeferenced using the ETRS89/UTM Zone 30 N projection system. To carry out both processes, it was necessary to use the Toolbox (S3TBX) under the open source software environment SNAP, version 9.0.0.

2.4.1. NDVI ^{THM} and PV

NDVI with Sentinel 2 imagery is determined by the red band (4) and the near-infrared spectral band (8). This index allows us to determine if there is vegetation upon a certain zone or area. The range of this index is between − 1 (clear soils and devoid of vegetation) and 1 (dense and thick vegetation). It is calculated by means of Eq. (1) (Shafizadeh-Moghadam et al., 2020):

$$NDVI = \frac{NIR - Red}{NIR + Red} \quad (1)$$

Next, the PV was calculated using Eq. 2 (Yu et al., 2014):

$$PV = \left[\frac{NDVI - NDVI_{\min}}{NDVI_{\max} - NDVI_{\min}}\right]^2 \quad (2)$$

where NDVI is the normalized vegetation index obtained by formula (1) and the NDVI max and NDVI min are the maximum and minimum values of the NDVI interval.

2.5. Sentinel 3 images

Tier 2 Sentinel 3 satellites allow for LST imaging at 1000-meter resolution using the high resolution scanning radiometer. NDVI and PV images can also be obtained —along with other associated parameters— directly and automatically at a resolution of 500 m. Granada lies beneath the path of satellites Sentinel 3 A and 3B. The first has a daily timetable that oscillates between 10:00 and 11:00 a.m.; the second passes between 9:00 p.m. and 10:00 p.m. The images chosen for the study correspond to the same ten days of the Sentinel 2 images. In this way, throughout the months of July and August of the year 2022, a total of 20 images could be used, 10 corresponding to Sentinel 3 A and another 10 to Sentinel 3B (Table 3).

The selected images correspond to periods of meteorological conditions considered normal. All of them have a cloudiness index of less than 5% in order to increase the accuracy in obtaining the LST and the subsequent calculation of the PCI and SUHI. After downloading the Sentinel 3 images, they were atmospherically corrected and georeferenced using the ETRS89/UTM Zone 30 N projection system. Both processes were carried out using the Toolbox (S3TBX) under the open source software environment SNAP, version 9.0.0.

2.6. Image reclassification using TsHARP algorithm

Along with the rise in observations of the Earth's surface made by remote sensing yet the low quality of the thermal images of Sentinel 3, there arose a need to generate processes to enhance their resolution. The sharpening methods developed include STARRFM, TsHARP and Distrad. They increase the resolution of Sentinel 3 and MODIS images with the help of Sentinel 2 images. Affording high precision despite its simplicity is the TsHARP method (Agam et al., 2007; Huryna et al., 2019; Zhou et al., 2020), based on the establishment of a linear regression model between the NDVI, PV and LST images of Sentinel 2 and Sentinel 3 through Eq. (3):

$$LST_{coarse} = a + b \times PV_{coarse} \quad (3)$$

where a and b are the linear regression coefficients, while PV_{coarse} and LST_{coarse} are the PV and LST obtained by Sentinel 3 at a resolution of 1000 m. Next, we use Eq. (4):

$$LST_{fine} = a + b \times PV_{fine,} \quad (4)$$

where a and b are the previously determined linear regression coefficients, PV_{fine} is the plant proportion obtained by Sentinel 2 at 10 m, and LST_{fine} is the new LST obtained at a resolution of 10 m. Finally, because it is a linear regression, it is essential to include the residual error obtained in the LST image to ensure the accuracy of the prediction. All this according to Eq. (5):

$$LST_{downscale} = LST_{fine} + Residual \quad (5)$$

2.7. Park cool island estimate

PCI can be defined as the temperature difference between urban areas and green areas taken at the same time (Oliveira et al., 2011)

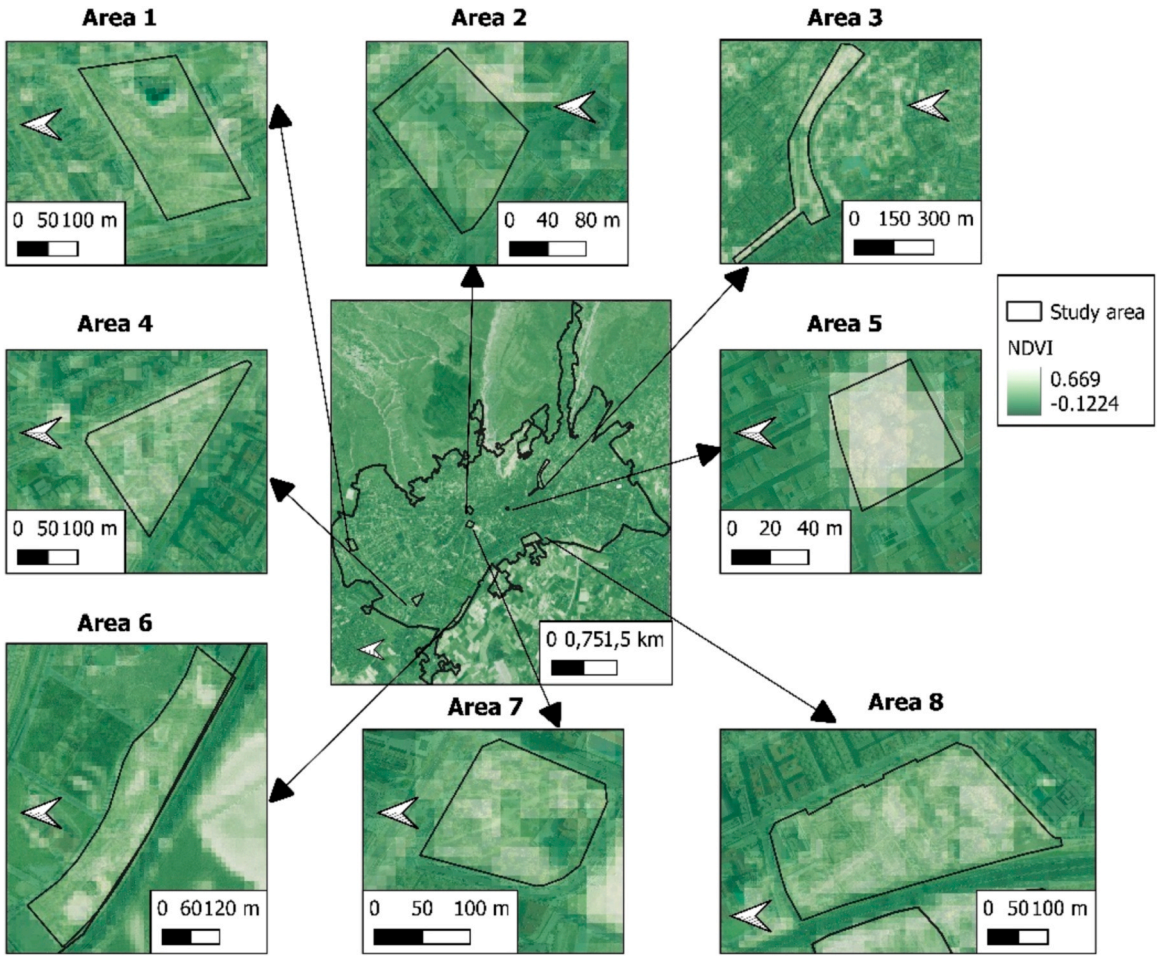

Fig. 4. NDVI index of the investigated areas.

according to Eq. (6):

$$PCI = LST_{parkland} - LST_{urban} \quad (6)$$

The LST values of the green areas were obtained using the statistics of QGIS software; they correspond to the mean values of the pixels included within the limit of each green area. The urban LST values correspond to the average values of the pixels located outside the boundary of the green areas in an environment of 500 m. This distance is sufficient to include the temperatures of buildings, streets and transport attached to green areas and has been used in previous studies (Lu et al., 2012; Saaroni et al., 2018). To determine the PCI, the raster calculator option of the open source software QGIS 3.22.10 was used.

2.8. Solar radiation

The solar radiation of each of the green areas investigated was obtained by means of simulations with the System for Automated Geoscientific Analysis (SAGA) software (Conrad et al., 2015). It allows for the incorporation of digital surface models thanks to the Light Detection and Ranging (LIDAR) program, which was downloaded from the official website of the National Geographic Institute of the Government of Spain. The use of these simulations within the scientific community is common and has been validated (Bremer et al., 2016; Zakšek et al., 2005). After the simulation, the findings were compared with the solar radiation data from the meteorological station of the State Meteorological Agency (AEMET) in Granada in order to determine the average precision error with respect to the station. It was 1%, well in line with those obtained in other simulation studies of solar radiation involving SAGA software (Bremer et al., 2016; Zakšek et al., 2005).

2.9. Wind and wind factor

Wind is considered an important factor in the study of the variability of SUHI and PCI in cities (Gaur et al., 2018; van Hove et al., 2015). This was simulated with the SAGA software and later compared with the data from the AEMET weather stations (Airport and Cartuja). These have a precision of ± (0.1 m/s + 1.5% of the V.M.) being able to report values that oscillate between 0.3 and 20 m/s. The graphic documentation obtained with SAGA (Conrad et al., 2015) presents a spatial resolution of 5 m, very suitable for studies on cities. The results obtained from the simulation were compared with those reported by the meteorological stations reporting coincident values in both speed and direction of the wind (Airport: R^2 =0.97 and Cartuja: R^2 =0.94). Next, the wind factor was obtained. which is a dimensionless value that depends on the speed and direction of the wind and that allows determining the effect of the average wind on urban areas from all directions. It was obtained by simulation with the SAGA software by introducing the speed and direction of the wind and the digital model of surfaces obtained by LIDAR (Olaya et al., 2009; Conrad et al., 2015). Values between 0 and 1 indicate areas with little or no wind, while values above 1 indicate areas highly exposed to wind.

2.10. Altitude

It is known by the scientific community that altitude affects urban climates and must be taken into account when evaluating SUHI and PCI

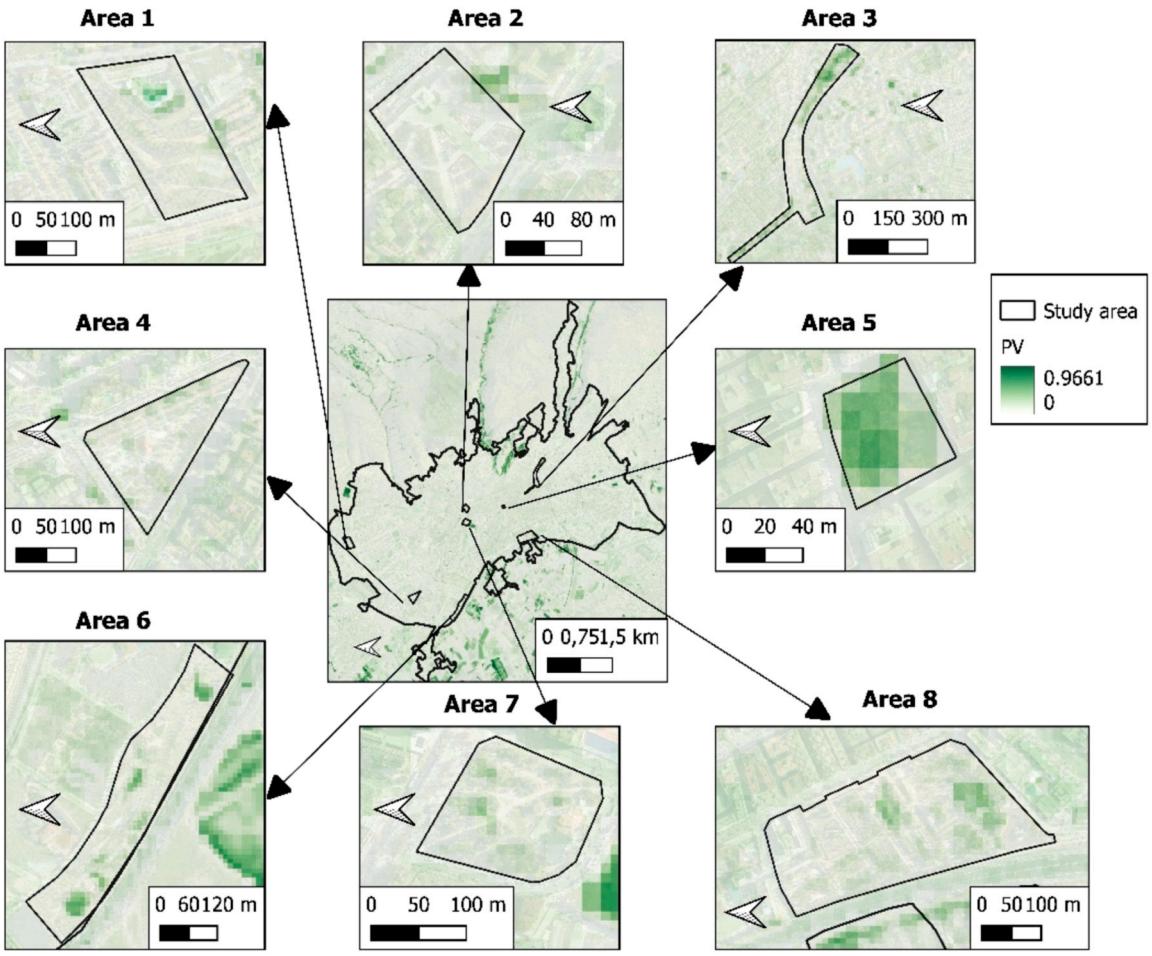

Fig. 5. PV index of the investigated areas.

Table 4
Statistics of the NDVI and PV by area.

	NDVI				PV			
Area	Max	Min	Mean	SD	Max	Min	Mean	SD
1	0.504	-0.112	0.251	0.093	0.527	0.006	0.062	0.074
2	0.500	0.038	0.195	0.090	0.197	0.003	0.058	0.041
3	0.594	0.051	0.334	0.133	0.614	0.001	0.155	0.132
4	0.481	0.082	0.302	0.081	0.306	0.007	0.078	0.057
5	0.585	0.133	0.473	0.105	0.581	0.047	0.341	0.158
6	0.576	0.071	0.291	0.105	0.553	0.003	0.089	0.110
7	0.511	0.042	0.278	0.107	0.376	0.005	0.084	0.066
8	0.542	0.044	0.302	0.100	0.453	0.003	0.091	0.086

Max: Maximum; Min: Minimum SD: Standard deviation.

(Gaur et al., 2018; Saaroni et al., 2018; Solecki et al., 2005). The mean altitude data for each area studied were obtained with QGIS from DEM data at 2 m (from the IGN).

2.11. SVF

The SVF is a parameter commonly used to determine the impact of urban forms on the LST, SUHI and PCI (Chun and Guldmann, 2014; Hidalgo and Arco, 2021; Hu et al., 2020). The SVF affects the possible heating and cooling of areas due to the vegetal and architectural elements that act as obstacles, such as: existing buildings, trees and vegetation. This variable is defined as the ratio between the visible area and the portion of the sky that is obstructed in a given area. Its value is dimensionless and varies between 1 and 0, the former indicating that solar radiation cannot expand into the atmosphere because the sky is completely blocked by obstacles, while the latter means that all radiation can expand freely into the atmosphere due to an absence of obstacles. To simulate the SVF of the areas under study, SAGA simulation software was used. The details of this process have been described by other authors (Dirksen et al., 2019; Hu et al., 2020; Zakšek et al., 2005). It was necessary to have the DEM and the digital surface map from IGN. Subsequently, the simulation was carried out in SAGA, and the mean values were exported to QGIS.

2.12. LSI

This variable is defined as the ratio between the real length of the perimeter of the green zone and its area. The value of a circle is 1, while the value of other shapes usually has a value greater than 1. It is commonly used in studies related to urban green infrastructure in urban

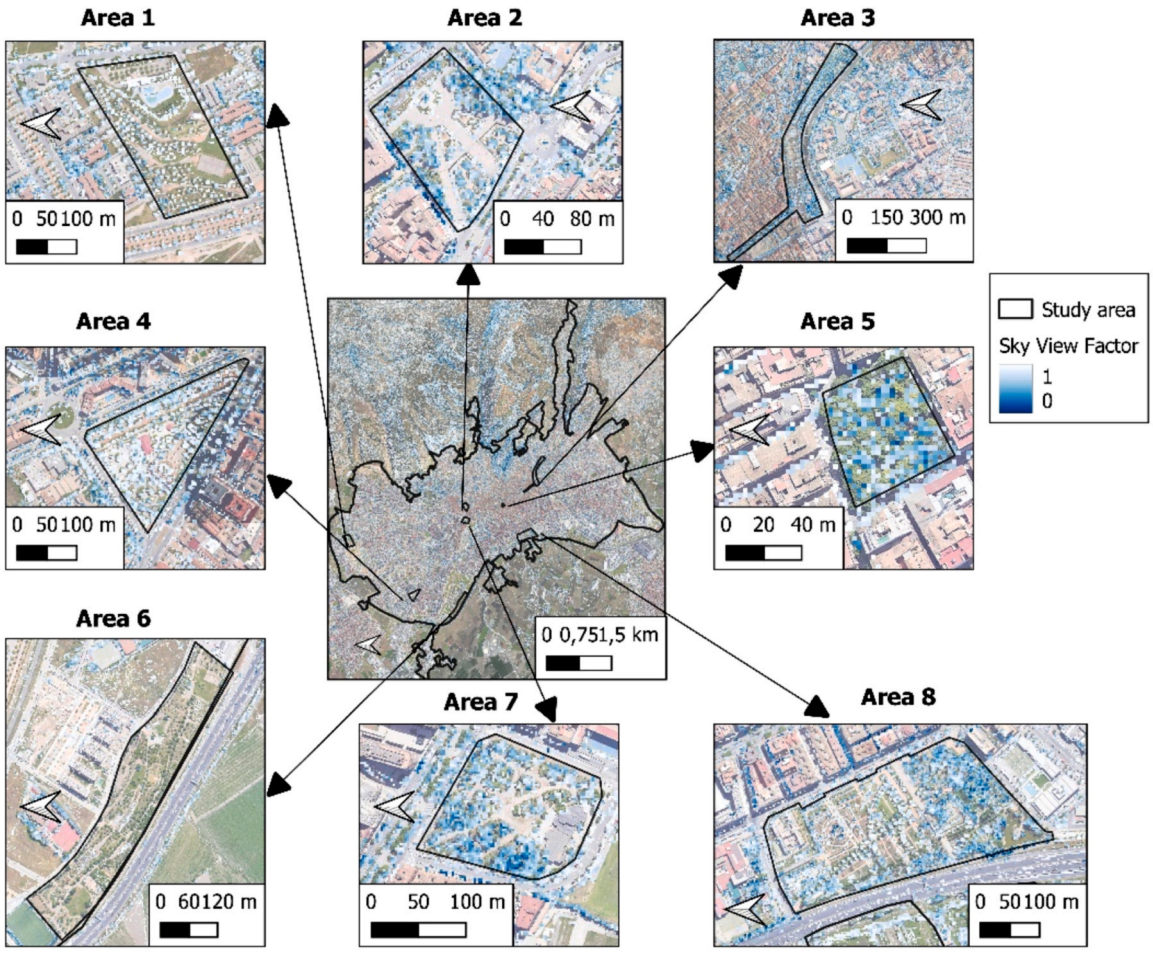

Fig. 6. SVF index of the investigated areas.

areas (Saaroni et al., 2018; Wu et al., 2019). It is calculated by the Eq. (7):

$$LSI = \frac{L}{2 \times \sqrt{\pi \times A}} \tag{7}$$

where L is the length of the entire perimeter of the investigated area and A is the area.

2.13. Strategy of analysis

Having data from various indices and variables on different green areas of the city of Granada as well as time series (July and August 2022), it was necessary to apply two methodologies: Analysis of variance (ANOVA) and Data Panel. The first statistical method allowed us to determine if there were statistically significant differences between the different green areas by comparing the variances. To this end, the ANOVA used a dependent variable (variables LST, SVF, DEM, NDVI and PV) and another independent variable (green areas). This methodology, well described in the literature on this type of study (Safarrad et al., 2021; Sharma et al., 2022), makes it possible to eliminate the possible sampling errors that plague studies of these characteristics. The Panel Data statistical analysis allows one to combine a dimension of data or values with a time dimension. It is frequently used in similar studies and involves the use of multiple regression models (Alcock et al., 2015; Chen et al., 2011; Fang and Tian, 2020), which means that a greater amount of data can be included than under traditional methods. The system establishes three calculation options: ordinary squares method (OSM), generalized least squares (GLS) and intragroup estimation method (IEM) (Labra, 2014). To calculate which methodology to follow, it is necessary to carry out the following steps (Chen et al., 2011): 1) Determine the effects of the analysis (random or fixed) using the Hausman test, to determine different hypotheses about the behavior of the residuals of the statistical analysis. 2) Using the Wooldridge and Wald tests, evaluate the model. These two phases will establish the most appropriate method to carry out (Seto and Kaufmann, 2003). Statistical analysis was performed with STATA software, version 16. For our research and after performing the indicated tests, the IEM method with random effects was used according to Eq. (8).:

$$Y_{it} = \beta \quad X_{it} + \alpha_i + \mu_{it} \tag{8}$$

where μ_{it} is the error of the model, α_i represents the individual effects, X_{it} are explanatory variables, and β is an independent variable.

3. Results

3.1. Space-time evaluation of the NDVI and PV indices

The space-time analysis of the NDVI and PV indices in the areas under study can be seen in Figs. 4 and 5. Table 4 gives the basic statistics of each of the areas investigated. The NDVI index makes it possible to differentiate areas of vegetation from artificial terrestrial areas without vegetation. In addition, it allows to know the vigor and state of the vegetation on the earth's surface. PV is defined as the percentage or fraction of occupation of vegetation canopy in a given ground area in vertical projection.

It is seen that the NDVI index presents an average value ranging from

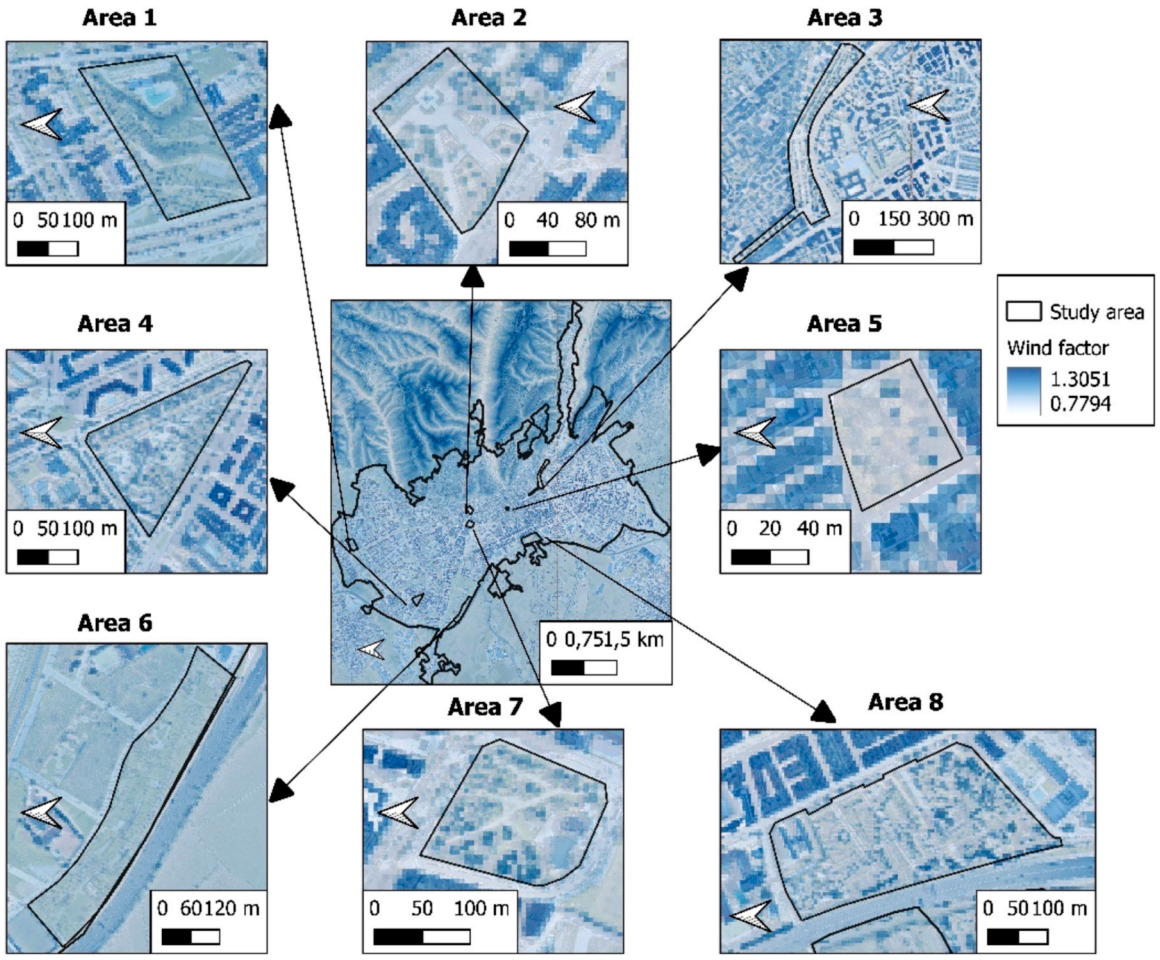

Fig. 7. Wind factor of the investigated areas.

the highest value (0.473) located in area 5 to the lowest (0.195) in area 2. The average value of the NDVI index of the green areas investigated was 0.303, while for urban areas it was 0.143. The green areas have a higher NDVI value than the urban areas of the city of Granada. The PV index presents an average value between the highest value (0.341), pertaining to area 5, and the lowest (0.058) in area 2. The spaces with greater and lesser PV index coincide with NDVI spaces. The average value of the PV index of the green areas investigated was 0.120, while for urban areas it was 0.102. The green areas were found to have a higher PV value than the urban areas of Granada. Taking into account that the selected satellite images correspond to July and August, the NDVI and PV values indicate that the vegetation of the studied area can be considered disperse and suitable for summertime.

3.2. LSI and DEM

The results of the LSI and DEM variables of the areas under study can be seen in Table 1. The value of LSI ranges between 2.5 in area number 3 and 1.1 in areas 2 and 7; the mean value of the LSI index was 1.43. The DEM value oscillates between area 1, which is located at the highest altitude (708 m), and area 6, located at the lowest altitude (643 m). The average altitude of the areas under study is 672 m.

3.3. SVF, wind factor and radiation

The space-time analysis of the variables SVF, wind factor and radiation of the areas under study are found in Figs. 6, 7 and 8. Table 5 shows the basic statistics of each of area investigated.

The SVF index is seen to present an interval that oscillates between the highest value (0.93) in area 6, and the lowest (0.62) located in area 5. The average value of the SVF index of the green areas investigated was 0.70, while for urban areas it was 0.75. The interval of the wind factor variable ranges from the highest value (1.00) located in area 1 to the lowest value (0.88) in area 5. The average value of the wind variable in the green zones investigated is 0.955, while that of urban areas is 0.899.

The interval of the solar radiation variable oscillates between the highest value (1893) pertaining to area 6, and the lowest (1507) in area 5. The average value of the radiation variable in the green areas studied is 1662, whereas that of the urban areas is 1579. A relationship between the variables SVF and radiation is seen, in that the higher the radiation, the lower the SVF, and vice versa.

3.4. LST

The space-time analysis of the day and night LST of the areas under study is presented in Figs. 9 and 10. Table 6 gives the basic statistics of the LST obtained.

The daytime LST is seen to oscillate a high (312.6 K) located in area 1 and a low (310.3 K) located in area 5. The average value of the daytime LST of all green areas investigated was 311.7 K; for urban areas it was 312.7 K. These values report a difference of 1.0 K between the two zones, the average daytime LST of the urban zones being higher. The mean daytime LST of the green areas with trees was lower (311.6 K) than the LST of the green areas with grass (312.5 K). The average nocturnal LST gives its highest value (296.4 K) for area 4 and the lowest (294.9 K) for area 5. The average value of the nocturnal LST of all the

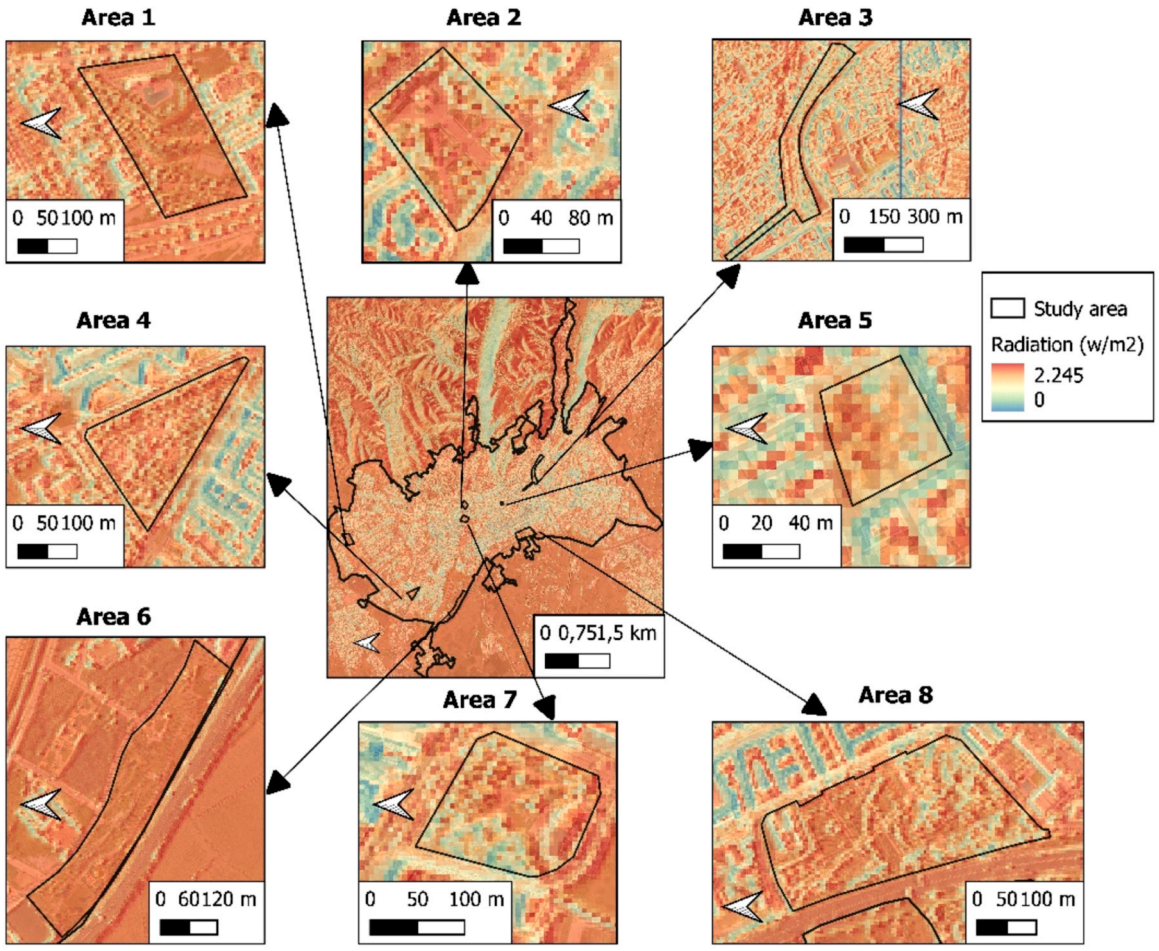

Fig. 8. Radiation of the investigated areas.

Table 5
Statistics of the SVF, wind factor and radiation by area.

	SVF				Wind factor				Radiation			
Area	Max	Min	Mean	SD	Max	Min	Mean	SD	Max	Min	Mean	SD
1	0.99	0.24	0.87	0.13	1.14	0.94	1.00	0.04	2177	1093	1837	159
2	0.98	0.10	0.69	0.19	1.11	0.86	0.94	0.05	2187	512	1710	334
3	0.99	0.11	0.57	0.20	1.21	0.80	0.93	0.11	2185	275	1343	275
4	0.99	0.18	0.81	0.14	1.17	0.88	0.99	0.06	2182	802	1746	255
5	0.99	0.14	0.62	0.19	1.11	0.83	0.88	0.05	2078	594	1507	308
6	0.99	0.27	0.93	0.11	1.17	0.91	0.98	0.02	2173	747	1893	089
7	0.99	0.08	0.65	0.19	1.17	0.85	0.96	0.07	2191	413	1596	375
8	0.99	0.02	0.70	0.20	1.21	0.85	0.96	0.08	2194	436	1664	332

Max: Maximum; Min: Minimum SD: Standard deviation.

green areas was 295.7 K, while for urban areas it was 296.3 K. These values mean a difference of 0.6 K between the two areas, the average nocturnal LST again being higher in urban areas than in green areas. The average nocturnal LST of the green areas with trees was greater (296 K) than the LST of the green areas with grass (295.5 K). In order to validate and determine the accuracy of the algorithm, the LST values obtained have been compared with the ambient temperature values of the two meteorological stations that the State Meteorological Agency has in the city of Granada. This methodology is gaining strength in recent years as a validation and verification system (Avdan et al., 2016; Rongali et al., 2018). The new LST presents a difference of 2.26 K with respect to the ambient temperature and a correlation coefficient of $R^2 = 0.9470$. These values are consistent and are within the limits reported by studies that compare both temperatures.

Fig. 11 shows the day and night LST of green areas classified into four types based on their surface area: type 1: $< 5000\ m^2$; type 2: between 5,000 and 20,000 m^2; type 3: between 20,000 m^2 and 70,000 m^2; and type 4: $> 70{,}000\ m^2$. In general terms, it is observed how both in the morning and at night, the LST of the green zones decreases as the surface of the green zone increases. That is, the larger the area of the green zone, the lower the LST value. However, during the mornings the green areas present lower LST in areas with more than 12,500 m^2, while at night the lowest LST values are reported in green areas of less than 12,500 m^2. The trend fits a 2nd degree polynomial graph with a linear fitting coefficients R^2.

3.5. PCI

The spatio-temporal analysis of the day and night PCI of the areas under study can be seen in Figs. 12 and 13. Table 7 shows the basic

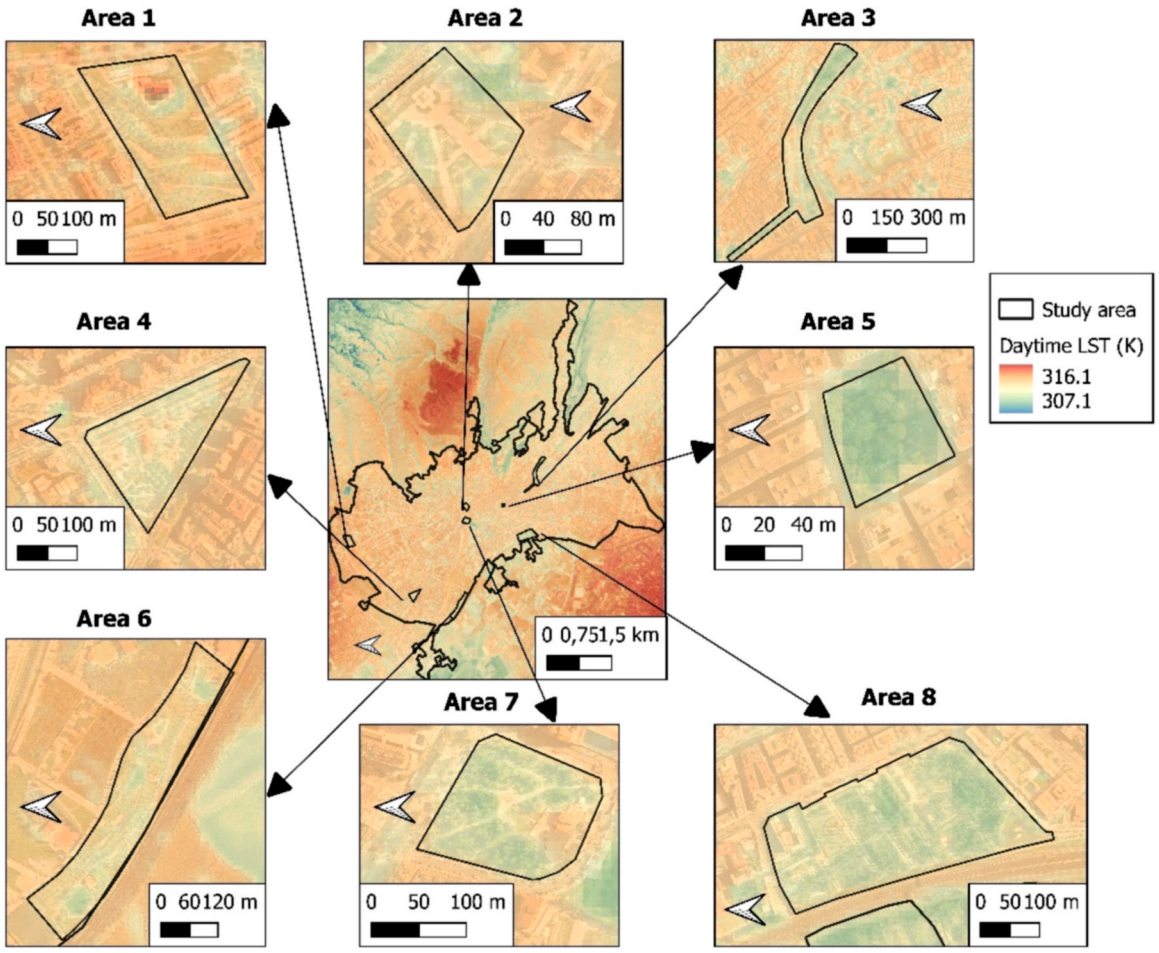

Fig. 9. Mean daytime LST of the investigated areas.

statistics of the day and night LST.

As can be seen, the daytime PCI with average values ranges from the highest value |4.5 K| of area 5 to the lowest value |2.2 K| of area 1. The average value of the daytime PCI of all green areas investigated was |3.2 K|.

Regarding the nocturnal PCI, it oscillates between the highest value |2.2 K| in zone 4 and the lowest value |0.8 K| in zone 5. The average value of the nocturnal PCI of all the green areas investigated was |1.5 K|.

Fig. 14 shows the day and night PCI (temperature differences) of the green areas according to the typologies indicated above: type 1: $< 5000\ m^2$; type 2: between 5000 and 20,000 m^2; type 3: between 20,000 m^2 and 70,000 m^2; and type 4: $> 70{,}000\ m^2$. In general terms, both in the morning and at night, the PCI of the green areas decreases as the area of the green area increases. Thus, the larger the area of green areas, the lower the PCI values, due to a smaller difference between the LST of green areas and the LST of urban areas. The trend lines fit a 2nd degree polynomial graph with a linear fitting coefficients R^2.

3.6. Effect extension

It is of great importance to analyze the distance to which the minimizing effect of green areas extends over day and night LST. To do this, two LST profiles (longitudinal 1–1′ and transverse 2–2′) were obtained for each of the investigated areas. Figs. 15 and 16 show the daytime and nighttime PCI profiles with a red line and the space occupied by the investigated areas with green shading. Fig. 15 shows the distance from the green area where the daytime LST is equal to the LST of the urban area, and therefore, the PCI obtains a value of 0. This distance is approximately between 30 and 150 m. Therefore, the minimization distance of the PCI is related to the surface of the green zone, so that the larger the surface, the greater the distance and vice versa. Fig. 16 illustrates how the distance at which the nighttime LST in the green zone equals the LST in the urban zone, ranging approximately between 60 and 120 m. A relationship between the distance and the area of the green zone is also observed. Accordingly, the greater the surface, the greater the distance; and vice versa. The distance is lesser at night than during the morning.

Fig. 17 shows the distance at which the day and night LST of the green areas equals the day and night LST of the adjoining urban areas. For this analysis, the classification of green areas made in the previous point was recovered (type 1: $< 5000\ m^2$; type 2: between 5000 and 20000 m^2; type 3: between 20000 m^2 and 70000 m^2 and type 4: $> 70000\ m^2$). In general, both in the morning and at night, the distances increase as the surface of the green area increases. The trend lines fit a 2nd degree polynomial graph with a linear fitting coefficients R^2. The distances are seen to be greater during the nights than during the mornings up to a green area surface of approximately 25000 m^2. From that point onward the distance is greater during the mornings.

3.7. Statistical analysis

3.7.1. ANOVA of the variables

The results of the ANOVA test carried out on the investigated variables reflected, through the Shapiro Wilk test, that they do not present normal distributions within the different green areas investigated, since P value < 0.05. Therefore, to continue with the ANOVA analysis for non-normal distributions, it is necessary to perform the Kruskal Wallis test. Therefore, and according to the reported results, the values of the

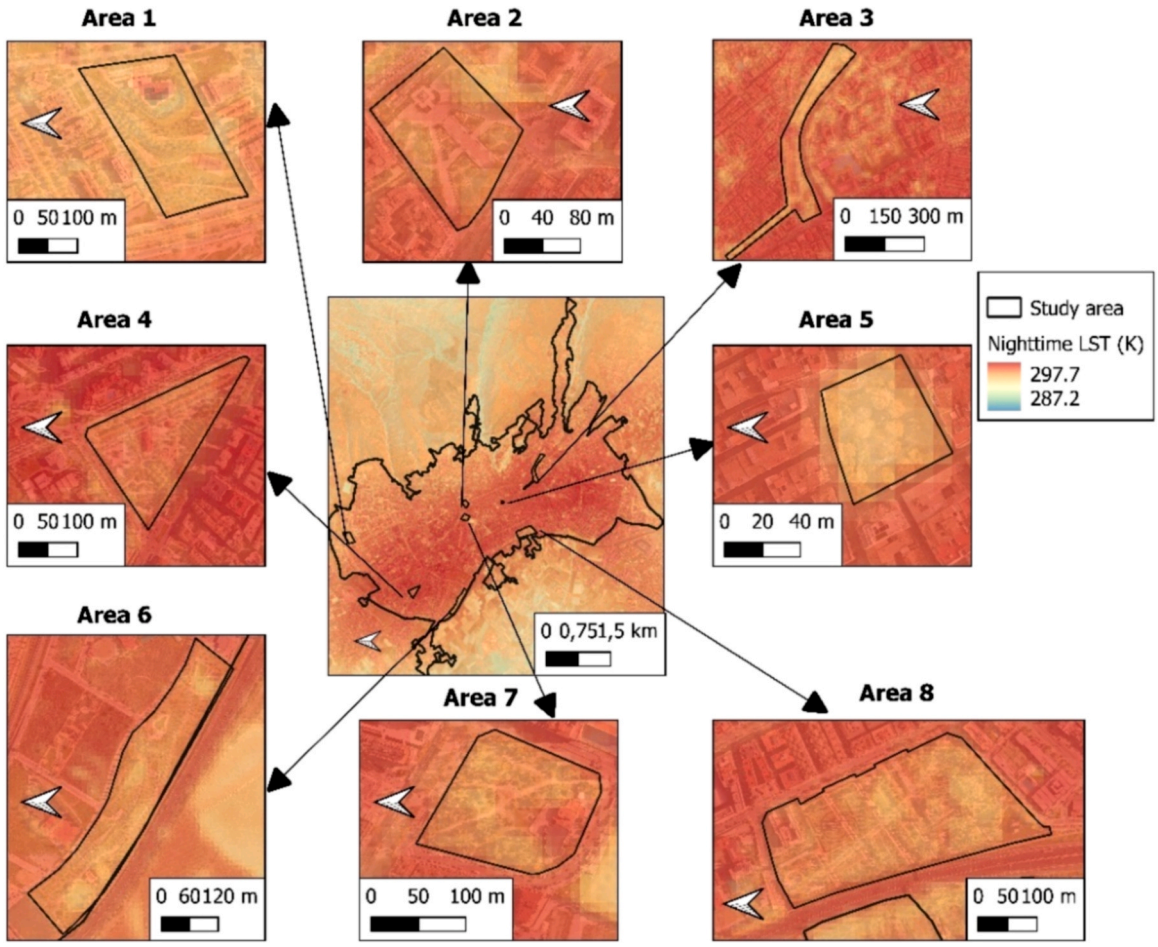

Fig. 10. Mean nighttime LST of the investigated areas.

Table 6
Statistics of the LST by area.

	LST daytime				LST nighttime			
Area	Max	Min	Mean	SD	Max	Min	Mean	SD
1	314.9	311.0	312.6	0.57	296.6	293.9	295.0	0.41
2	313.0	310.2	312.1	0.50	296.7	294.8	296.0	0.36
3	312.9	309.6	311.2	0.56	297.1	294.3	295.7	0.63
4	312.9	311.2	311.9	0.34	297.1	295.7	296.4	0.27
5	312.2	309.5	310.3	0.59	295.8	294.3	294.9	0.42
6	313.3	310.7	312.1	0.47	296.5	294.5	295.7	0.38
7	312.9	310.3	311.5	0.58	297.0	295.0	296.0	0.44
8	312.6	309.9	311.3	0.51	296.8	294.8	295.8	0.39

Max: Maximum; Min: Minimum; SD: Standard deviation.

variables NDVI, PV, LSI, DEM, wind, radiation and SVF present statistically significant relationships above 99% among the different green areas investigated. To the contrary, the LST and PCI variables do not present any statistically significant relationship between the different areas investigated.

3.7.2. *PCI and investigated variables*

In order to determine the relationships between day and night PCI and the rest of the variables studied, statistical analysis was carried out using the Data Panel method. To do this, first the Pearson correlation coefficient was determined. To apply the Data Panel, the Generalized Least Squares (GLS) method was used through Eq. (8). The results of the analysis are indicated in Tables 8, 9 and 10. Table 8 indicates that the daytime PCI presents a strong positive correlation with LST (0.903) and LSI (0.246) and an inverse correlation with the NDVI (−0.564) and DEM (−0.180) indices. Note the strong negative correlation between the SVF variable and the radiation received (−0.923).

As seen in Table 9, the nocturnal PCI presents a strong positive correlation with LST (0.929) and LSI (0.195), and an inverse correlation with the NDVI indices (−0.418). Note the strong negative correlation between the SVF variable and the radiation received (−0.923).

The results of statistical analysis using the Data Panel technique (Table 10) report that during the mornings there is a statistically significant and positive relationship above 99% between the PCI and LST and DEM variables, negative above 99% with the NDVI and PV variables and positive of 95% with the solar radiation variable. During the nights, there is a statistically significant and positive relationship between the PCI and LST variables, negative above 99% with the LSI and radiation variables, positive of 99% with the SVF variable, and negative of 95% with the NDVI and PV variables. During the mornings, the NDVI, PV and DEM variables have a strong relationship with the PCI, lowering it significantly during the nights. Contrariwise, at night the LSI, SVF and radiation variables are the ones that present a greater relationship. In both cases, a good concordance is observed between the dependent variable and the independent ones, given the values of R^2, F and Prob>Chi^2. The adjustment level is greater than 99% significance since Prob>Chi^2 = 0.000. These results are in line with the analytical values obtained above.

3.7.3. *Minimizing effect distance and variables*

In order to determine the relationships between the attenuation distance and the rest of the variables studied, statistical analysis was carried out using the Data Panel method (as described in the previous

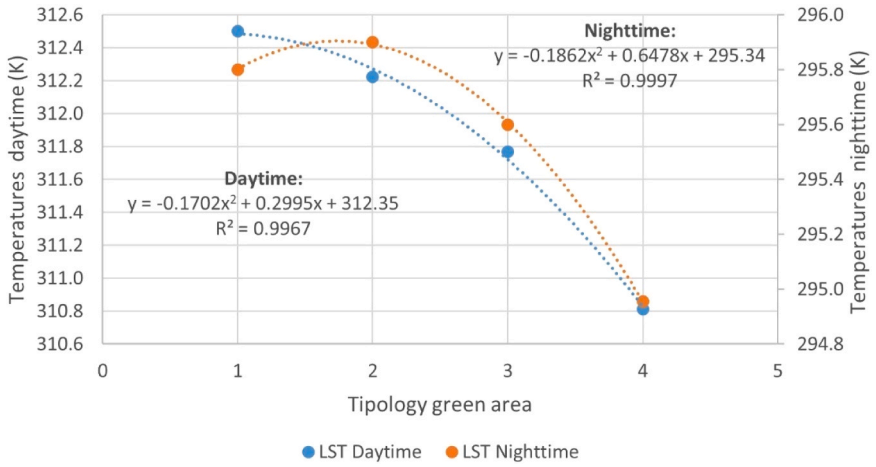

Fig. 11. Daytime and nighttime average LST by type of green areas.

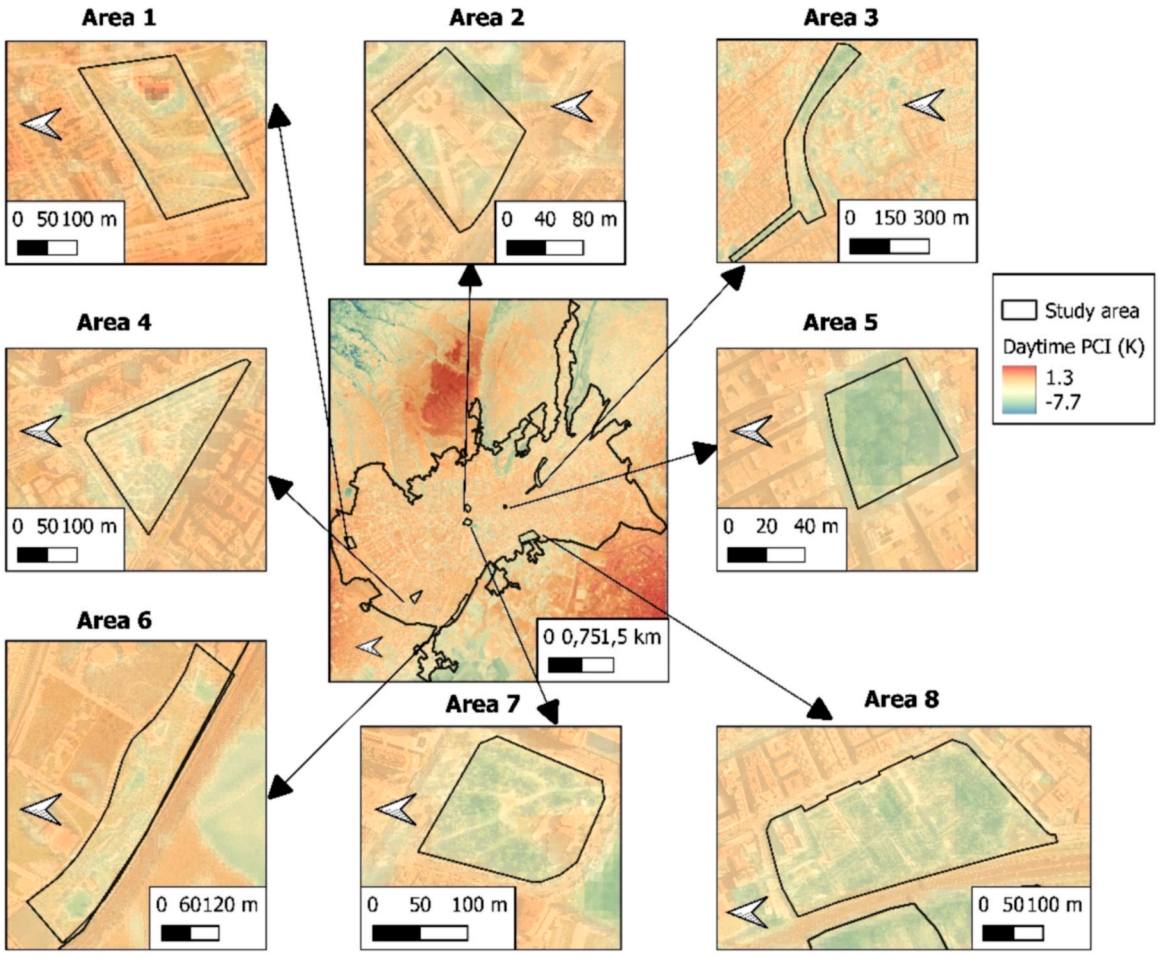

Fig. 12. Mean daytime PCI of the investigated areas.

point). The results are indicated in Tables 11, 12 and 13.

As seen in Table 11, the attenuation distance presents a strong positive correlation with LSI (0.5952) and Wind (0.3182) but an inverse correlation with the NDVI index (−0.112). Table 12 shows, in turn, that the night distance presents a strong positive correlation with PV (0.2598) and LSI (0.3698) and an inverse correlation with the DEM index (−0.1016).

The results of the statistical analysis using the Data Panel technique (Table 13) report that during the mornings there is a statistically significant and positive relationship above 99% among the distance variable and the NDVI, PV, LSI and wind variables, and negative above 99% with the variable DEM. During the nights, there is a statistically significant and positive relationship over 99% between the distance variable and NDVI, LSI and wind, negative over 99% with the DEM variables, positive over 99% with the radiation variable, negative and 99% with the SVF variable, and 95% positive with the PV variable. During the

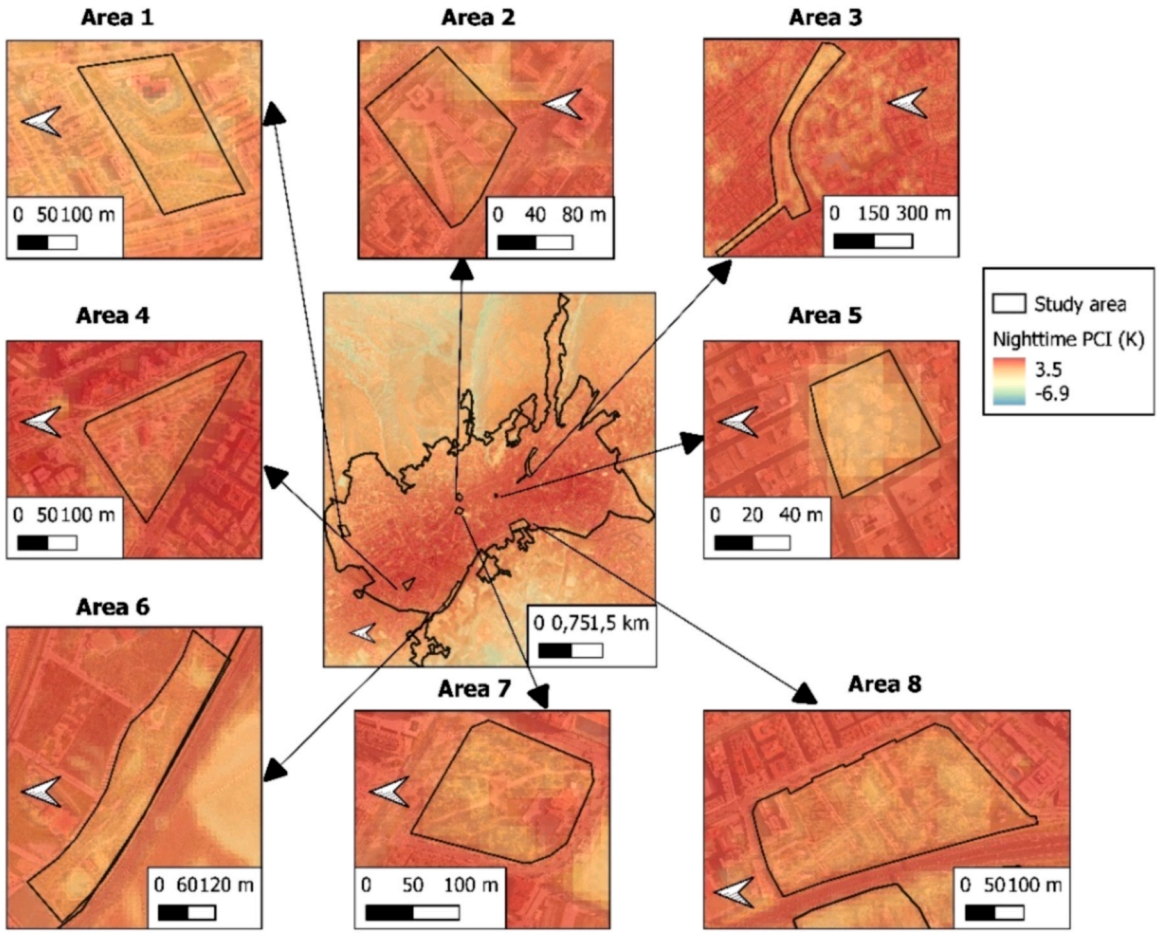

Fig. 13. Mean nighttime PCI of the investigated areas.

Table 7
Statistics of the PCI by area.

	PCI daytime				PCI nighttime			
Area	|Max|	|Min|	|Mean|	SD	|Max|	|Min|	|Mean|	SD
1	0.1	3.8	2.2	0.57	2.5	0.3	0.9	0.41
2	1.8	4.6	2.7	0.51	2.6	0.7	1.9	0.37
3	1.9	5.2	3.6	0.75	2.9	0.2	1.5	0.63
4	1.9	3.6	2.9	0.34	2.9	1.6	2.2	0.27
5	2.7	5.3	4.5	0.59	1.6	0.2	0.8	0.42
6	1.6	4.1	2.7	0.46	2.3	0.3	1.5	0.38
7	1.9	4.5	3.3	0.58	2.8	0.8	1.7	0.44
8	2.3	4.9	3.6	0.51	2.6	0.6	1.6	0.38

|Max|: Absolute maximum values; |Min|: Absolute minimum values; SD: Standard deviation.

mornings, the variables NDVI, PV, LSI, DEM and wind show a strong relationship with distance. On the contrary, at night the NDVI, LSI, DEM and wind variables are the ones that present a greater relationship. In both cases, it is observed that there is a good agreement between the dependent variable and the independent ones, reflected in the values of R^2, F and Prob>Chi^2.

4. Discussion

This study analyzed the space-time variability of the LST and PCI during the months of July and August of the year 2022 in the city of Granada and its relationship with the NDVI, PV, LSI, DEM, SVF, wind and radiation indices. The objective of this research is to analyze the space-time variability of the PCI on 8 green spaces of different sizes in the city of Granada (Spain) and determine what factors might influence the cooling distance. All this in order to improve decision-making in the construction of future green areas in urban areas.

In the green areas studied, the NDVI and PV indices related to the vegetation present higher values than in the urban areas. On the other hand, the daytime and nighttime LST values of green areas are lower than those obtained in urban areas. However, PCI values during the day are higher in green areas, while at night they are lower. These values suggest that green areas produce a minimizing effect on the LST, and should therefore be considered as fundamental infrastructures for mitigating temperatures. Numerous studies using satellite images have shown a negative correlation between vegetation and temperatures, in that vegetation produces a cooling effect in urban areas (Du et al., 2020; Masoudi et al., 2021; Qiu et al., 2017) ranging roughly between 1.5 and 3.5 K (Lin et al., 2015; Saaroni et al., 2018). These effects are attributed to the shade produced by trees, as well as the evapotranspiration process and the rates of cooling and heating by convection and transpiration that modify the LST of the areas and would explain the day and night behavior of the PCI (Feizizadeh and Blaschke, 2013; Hidalgo and Arco, 2021; Zakšek et al., 2005). Our findings come to corroborate those of previous studies, showing that an increase in urbanized and impervious areas causes an increase in LST, while increases in green areas lead to a decrease (Saaroni et al., 2018; Wu et al., 2019).

A relationship appeared between the surface area of the green areas and the cooling distance around the area, but not with the decrease in temperatures they generate. It is logical to think that the greater the surface of a green area, the greater its cooling effect and the greater the cooling distance with respect to the green area, as previous authors point out (Chen and Wong, 2006; Lee et al., 2009; Lin et al., 2015; Saaroni

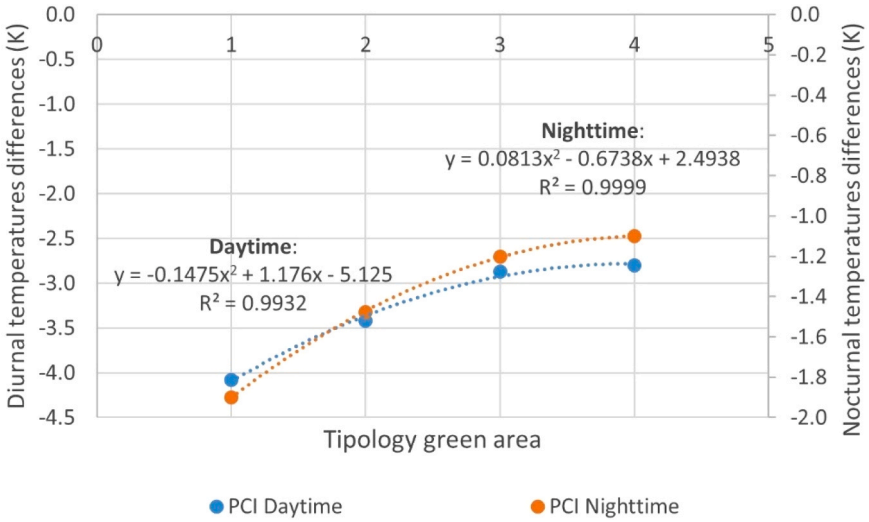

Fig. 14. Daytime and nighttime average PCI (temperature differences) by type of green areas.

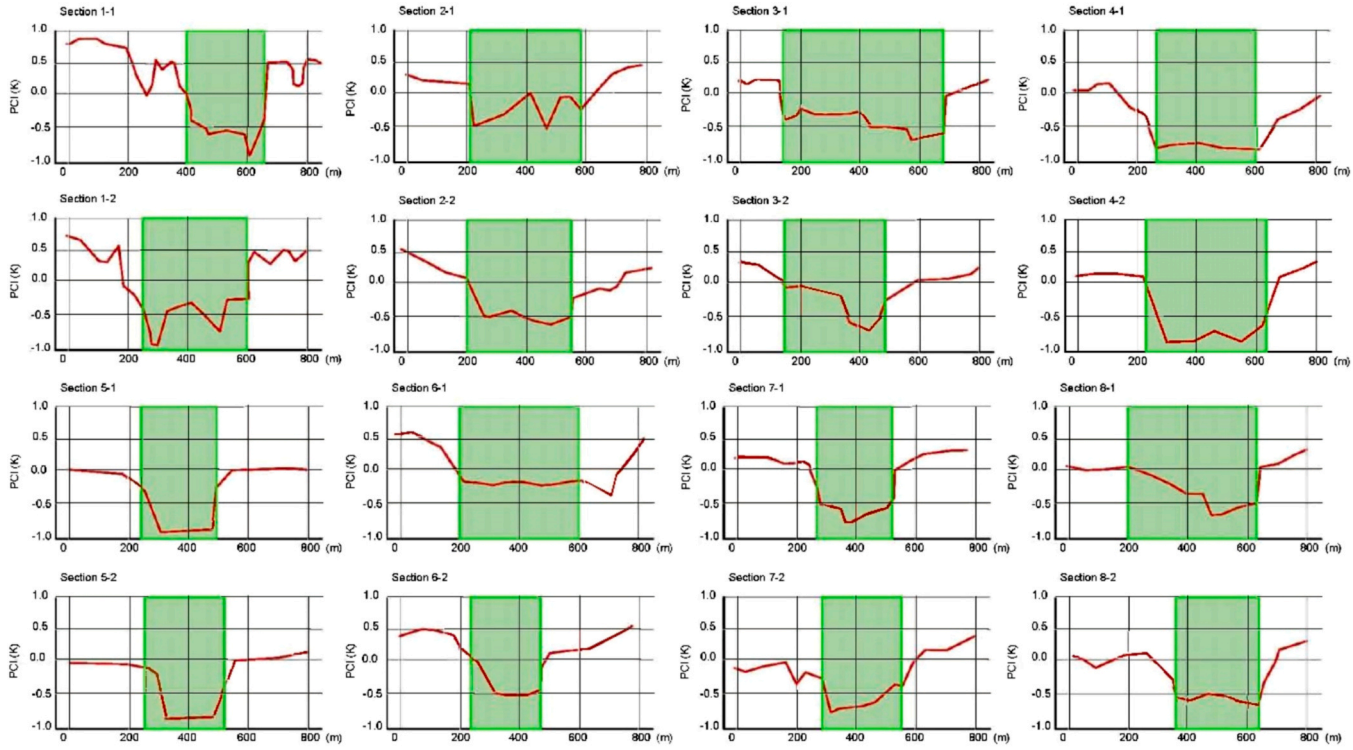

Fig. 15. Average diurnal PCI profiles of the areas under study.

et al., 2018; Upmanis et al., 1998; Yoshida et al., 2015). Our results report that the larger the surface area of the green area, the smaller the cooling effect it produces. This circumstance is controversial since it differs from the studies indicated above but could be motivated by the heat transferred from the vegetation to the atmosphere, which produces an increase in environmental temperature (Berendse, 2005; Shaver et al., 2000). The vegetation has a rough surface and a high albedo, which means that it receives significant solar radiation. In this way, at times of high temperatures, the vegetation increases the exchange of energy between the vegetation and the atmosphere, which implies an increase in evapotranspiration and a decrease in soil moisture, which produces an increase in the flow of heat. sensitive to the atmosphere (Shaver et al., 2000). Therefore, the greater the extension of green spaces and in conditions of high temperatures, the less minimization of the ambient temperature. Our statistical analysis shows that the variables NDVI, PV, LSI, DEM and wind have a strong relationship with distance both in the morning and at night. Indeed, at night, radiation and SVF are included as important variables. However, our LST minimization results for green areas lie below the average values obtained in other investigations carried out. For example, the city of Shenzhen (China) reported reductions of between 0.9 and 1.57 K (Qiu et al., 2017), the city of Mumbai (India) had reductions of between 2 and 3 K (Dwivedi and Mohan, 2018), and Singapore obtained reductions of between 1 and 3 K (Masoudi et al., 2021). In turn, our cooling distances are also well below those reported elsewhere: Seoul (Lee et al., 2009) gave a distance of 240 m, Singapore (Chen and Wong, 2006) a distance of 500 m, and for some green spaces in Gothenburg (Upmanis et al., 1998) a distance of 1000 m was detected. It is evident that the reduction of LST

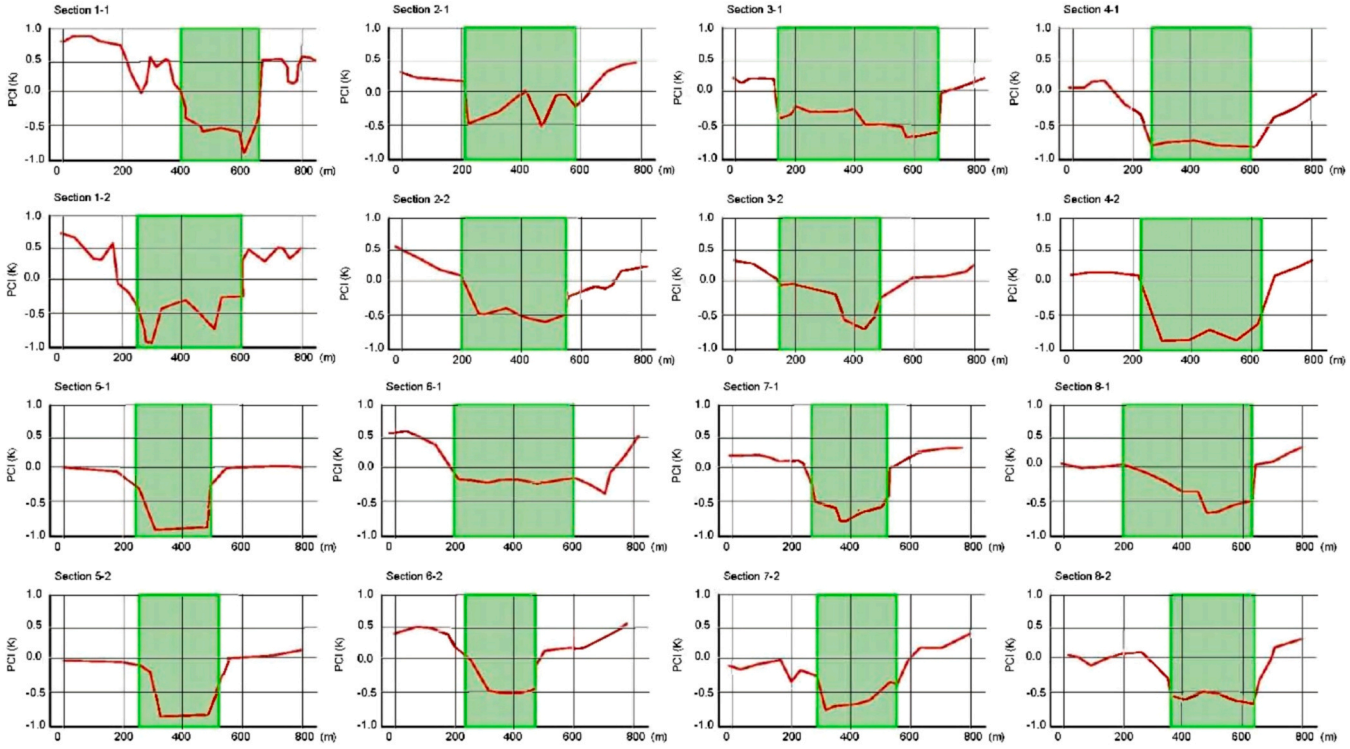

Fig. 16. Average nocturnal PCI profiles of the areas under study.

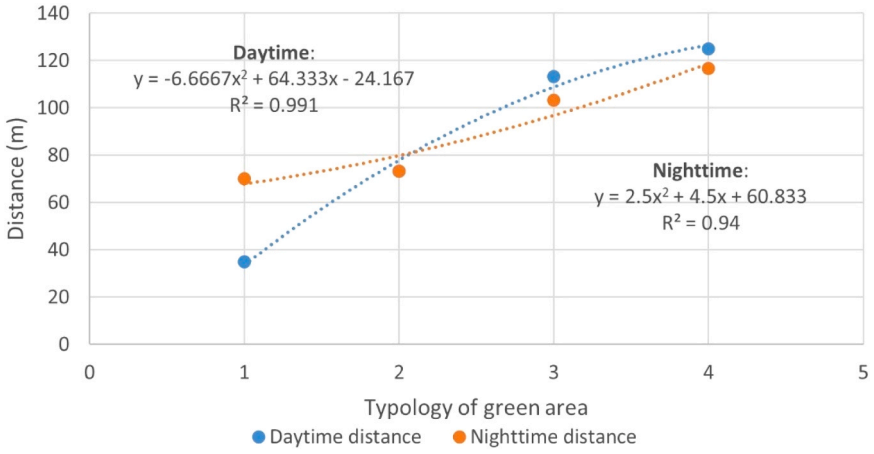

Fig. 17. Average diurnal LST profiles of the areas under study.

Table 8
Pearson's correlation coefficient and ρ value between daytime PCI and variables.

	PCI	LST	NDVI	PV	LSI	DEM	SVF	Wind	Radiation
PCI	1								
LST	*0.903* * **	1							
NDVI	*-0.564* *	-0.458	1						
PV	-0.054	-0.072	*0.601* * *	1					
LSI	*0.246* * *	0.040	*-0.407* *	0.000	1				
DEM	*-0.180* * *	-0.016	0.290	*0.550* * *	0.103	1			
SVF	0.148	0.096	-0.446	*-0.574* * *	-0.047	-0.388	1		
Wind	0.154	0.033	0.069	-0.033	-0.125	*0.427* *	0.368	1	
Radiation	0.068	0.084	*-0.431* *	*-0.578* * *	-0.303	-0.484	*-0.923* * *	0.255	1

Robust standard errors: *$p < 0.05$, * *$p < 0.01$ and * **$p < 0.001$.

Table 9
Pearson's correlation coefficient and ρ value between nocturnal PCI and variables.

	PCI	LST	NDVI	PV	LSI	DEM	SVF	Wind	Radiation
PCI	1								
LST	*0.929* * **	1							
NDVI	*-0.418* *	*-0.443* *	1						
PV	-0.062	-0.062	*0.601* * *	1					
LSI	*0.195* * *	0.044	*-0.407* *	0.000	1				
DEM	0.074	-0.073	0.289	0.549	0.103	1			
SVF	-0.117	0.034	*-0.446* *	*-0.574* *	-0.047	-0.388	1		
Wind	-0.064	-0.038	0.069	-0.032	-0.125	0.427	0.368	1	
Radiation	-0.146	0.036	*-0.430* *	*-0.578* * *	-0.303	*-0.488* *	*-0.923* * **	0.254	1

Robust standard errors: *p < 0.05, * *p < 0.01 and * **p < 0.001.

Table 10
Data Panel results for PCI and NDVI, PV and LULC indices.

	Daytime			Nighttime		
Variables	β	ρ	sd	β	ρ	sd
LST	0.1916	*0.000* * **	0.0058	0.3128	*0.000* * **	0.0055
NDVI	-3.8047	*0.000* * **	1.0189	-2.2781	*0.021* *	0.9908
PV	-1.1096	*0.000* * **	0.0860	-1.4029	*0.012* *	0.5592
LSI	0.0425	*0.661*	0.0970	-0.1137	*0.000* * **	0.0096
DEM	0.0147	*0.000* * **	0.0001	0.0045	0.262	0.0040
SVF	3.5999	*0.081*	2.0663	-0.6238	*0.009* * *	0.5019
Wind	0.2503	*0.494*	0.3661	0.3234	0.747	1.0008
Radiation	-0.0015	*0.019* *	0.0006	-0.0011	*0.000* * **	0.0009
	$R^2 = 0.82$	*F= 36454*	Prob>chi^2 = 0.000	$R^2 = 0.92$	*F= 45123*	Prob>chi^2 = 0.000

β: Coefficient; sd: Standard deviation; Robust standard errors: *p < 0.05, * *p < 0.01 and * **p < 0.001. R^2: Linear regression coefficient. F: F Statistic.

Table 11
Pearson's correlation coefficient and p value between diurnal distance and variables.

	Distance	NDVI	PV	LSI	DEM	SVF	Wind	Radiation
Distance	1							
NDVI	*0.1120* *	1						
PV	0.1606	*0.6096* * *	1					
LSI	*0.5952* * *	*-0.2699* *	0.0722	1				
DEM	0.0948	0.4010	*0.5980* * *	0.0169	1			
SVF	0.1175	*-0.4340* *	*-0.5771* * *	-0.1207	-0.4207	1		
Wind	*0.3182* *	0.2112	0.0055	-0.3178	0.3979	0.3517	1	
Radiation	-0.0706	*-0.4656* *	*-0.5923* * *	-0.3505	*-0.4942* * **	0.9288	0.2643	1

Robust standard errors: *p < 0.05, * *p < 0.01 and * **p < 0.001.

Table 12
Pearson's correlation coefficient between nocturnal distance and variables.

	Distance	NDVI	PV	LSI	DEM	SVF	Wind	Radiation
Distance	1							
NDVI	0.1013	1						
PV	*0.2598* * *	*0.6096* * *	1					
LSI	*0.3698* * *	*-0.2699* *	0.0722	1				
DEM	*-0.1016* *	0.4010	0.5980	0.0169	1			
SVF	-0.0164	*-0.4380* *	*-0.5771* * *	-0.1207	-0.4207	1		
Wind	0.0761	0.2112	0.0055	-0.3108	*0.3979* *	0.3517	1	
Radiation	-0.0496	*-0.4656* *	*-0.5923* * *	-0.3505	-0.4942	*0.9288* * **	0.2643	1

Robust standard errors: *p < 0.05, * *p < 0.01 and * **p < 0.001.

and cooling distance in the mentioned cities would be greater than those we reported; It is evident that the cities reviewed are large in size and population that have large green areas, not comparable to the small city of Granada. However, and seeing our results, this circumstance by itself would not justify this circumstance. It would be necessary to take into account both the latitude of the green spaces analyzed and the maximum environmental temperatures that they can reach in warm periods. If these are very high, the minimization of temperatures stagnates even though the size of the green zone increases as has been reported. This discrepancy has been verified in other investigations (Lin et al., 2015; Lu et al., 2012) reaching the hypothesis reviewed here. Thus, for example, the study on 4 green areas in the city of Wroclaw (Poland) reported a LST minimization distance of between 110 and 295 m (Blachowski and Hajnrych, 2021), while the study on 29 green areas cities in China, reported that in small cities, the cooling distance did not exceed 300 m. Finally and close to the city under study, Madrid (Spain), reported a distance of between 130 and 280 m (Aram et al., 2020). These studies are in line with the results reported in our research and could transfer a possible relationship between the size of cities and that of green areas.

The fact that a lower daytime LST was observed in green areas having trees as opposed to green areas with large expanses of grass, and vice versa at night, has been previously reported (Brown et al., 2015;

Tablee 13
Data Panel results between distance and variables.

	Daytime			Nighttime		
Variables	β	ρ	sd	β	ρ	sd
NDVI	51.515	*0.000* * **	6.3216	95.063	*0.000* * **	25.3178
PV	140.66	*0.000* * **	6.3792	112.080	*0.015* *	46.1655
LSI	34.553	*0.000* * **	1.4218	32.9617	*0.000* * **	2.5952
DEM	-0.7223	*0.000* * **	0.0254	-0.71265	0.000 * **	0.1153
SVF	-157.11	*0.165*	113.27	-437.036	*0.002* * *	143.266
Wind	697.33	*0.000* * **	54.282	426.525	0.000 * **	36.7496
Radiation	0.0773	*0.221*	0.0632	0.27327	*0.002* * *	0.0894
	$R^2 = 0.76$	*F= 12320*	Prob>chi^2 = 0.000	$R^2 = 0.92$	*F= 45123*	Prob>chi^2 = 0.000

β: Coefficient; sd: Standard deviation; Robust standard errors: *p < 0.05, * *p < 0.01 y * **p < 0.001. R^2: Linear regression coefficient. F: Statistical

Spronken-Smith, 2010; Yoshida et al., 2015). It is due to the shade produced by trees in the morning, which minimize the solar radiation received and therefore the LST. At night, heat from the ground tends to move into the atmosphere. If there is an area of trees with large vegetation, it makes the SVF small, so the heat is retained for a longer time between the ground and the treetops and therefore, the temperature of that area is maintained for a longer time. and zone cooling is delayed. This circumstance has been studied by other authors (Chun and Guldmann, 2014; Hidalgo and Arco, 2021; Zakšek et al., 2005), reaching conclusions similar to those reported here.

5. Conclusions

In recent years, the study of PCI and the cooling effect of green areas as mitigation measures for LST and SUHI in urban areas has become consolidated as a very important field of research. There is a dire need to know what elements alter urban climates in order to establish mitigation measures in the framework of future urban proposals, to improve the quality of life of citizens by increasing environmental comfort.

Based on the results obtained in our research, it can be concluded that there exists a relationship between the surfaces of green areas in urban areas, the decrease in temperatures they generate, and the cooling distance around the area. Accordingly, the area around the green zone that benefits from the cooling effect is greater as the surface of the green zone increases. Furthermore, green areas with trees have lower LST in the morning than green areas without trees, while an inverse effect occurs at night.

The method carried out in this investigation, which is based on high-resolution Sentinel 3 satellite images, is feasible to determine the extent of cooling. It does not require complicated on-site measurements and satellite images are free and easily accessible. To maximize the mitigation effects on the LST of cities, we can conclude that it is recommended to have green areas and, in cases where possible, increase their surfaces, preferably with grass and tree floors that do not imply an SVF greater than 0.8. At the same time, and when this is not possible due to the already built urban configuration, it is necessary to naturalize the streets. For this, it is necessary to transform the spaces by reducing the areas for vehicles and increasing the circulation areas for pedestrians and bicycles with an important integration of green areas and trees.

Such findings provide new evidence of the correlation between the LST, SUHI and PCI in urban areas and green areas. This knowledge is helpful for urban planning and management, and for the establishment of guidelines for public administrations. In short, new green areas in urban areas ultimately make them more resilient to increases in LST and climate change.

Funding

This research was funded for the open access charge: Universidad de Granada, CBUA.

CRediT authorship contribution statement

David Hidalgo García: Conceived and designed the analysis, Collected the data, Contributed data or analysis tools, Performed the analysis, Wrote the paper, Other contribution.

Declaration of Competing Interest

The authors declare that they have no known competing financial interests or personal relationships that could have appeared to influence the work reported in this paper.

References

Agam, N., Kustas, W.P., Anderson, M.C., Li, F., Neale, C.M.U., 2007. A vegetation index based technique for spatial sharpening of thermal imagery. Remote Sens. Environ. 107 (4), 545–558. https://doi.org/10.1016/j.rse.2006.10.006.

Alcock, I., White, M.P., Lovell, R., Higgins, S.L., Osborne, N.J., Husk, K., Wheeler, B.W., 2015. What accounts for "England's green and pleasant land"? A panel data analysis of mental health and land cover types in rural England. Landsc. Urban Plan. 142, 38–46. https://doi.org/10.1016/j.landurbplan.2015.05.008.

An, N., Dou, J., González-Cruz, J.E., Bornstein, R.D., Miao, S., Li, L., 2020. An observational case study of synergies between an intense heat wave and the urban heat island in Beijing. J. Appl. Meteorol. Climatol. 59 (4), 605–620. https://doi.org/10.1175/JAMC-D-19-0125.1.

Anjos, M., Targino, A.C., Krecl, P., Oukawa, G.Y., Braga, R.F., 2020. Analysis of the urban heat island under different synoptic patterns using local climate zones. Build. Environ. 185. https://doi.org/10.1016/j.buildenv.2020.107268.

Aram, F., Higueras, E., Solgi, E., Mansournia, S., 2020. Urban green space cooling effect in cities. Heliyon 5 (4). https://doi.org/10.1016/j.heliyon.2019.e01339.

Arbuthnott, K.G., Hajat, S., 2017. The health effects of hotter summers and heat waves in the population of the United Kingdom: a review of the evidence. Environ. Health.: A Glob. Access Sci. Source 16, 1–13. https://doi.org/10.1186/s12940-017-0322-5.

Avdan, U., Jovanovska, G., 2016. Algorithm for automated mapping of land surface temperature using LANDSAT 8 satellite data. J. Sens. 1–8. https://doi.org/10.1155/2016/1480307.

Blachowski, J., Hajnrych, M., 2021. Assessing the cooling effect of four urban parks of different sizes in a temperate continental climate zone: Wroclaw (poland. Forest 12 (8). https://doi.org/10.3390/f12081136.

Belgiu, M., Stein, A., 2019. Spatiotemporal image fusion in remote sensing. Remote Sens. 11 (7) https://doi.org/10.3390/rs11070818.

Berendse, F., 2005. Impacts of global change on plant diversity and vice versa: old and new challenges for vegetation cientists. J. Veg. Sci. 16, 613–616.

Bremer, M., Mayr, A., Wichmann, V., Schmidtner, K., Rutzinger, M., 2016. A new multi-scale 3D-GIS-approach for the assessment and dissemination of solar income of digital city models. Comput., Environ. Urban Syst. 57, 144–154. https://doi.org/10.1016/j.compenvurbsys.2016.02.007.

Brown, R.D., Vanos, J., Kenny, N., Lenzholzer, S., 2015. Designing urban parks that ameliorate the effects of climate change. Landsc. Urban Plan. 138, 118–131. https://doi.org/10.1016/j.landurbplan.2015.02.006.

Čeplová, N., Kalusová, V., Lososová, Z., 2017. Effects of settlement size, urban heat island and habitat type on urban plant biodiversity. Landsc. Urban Plan. 159, 15–22. https://doi.org/10.1016/j.landurbplan.2016.11.004.

Chen, Y., Li, X., Zheng, Y., Guan, Y., Liu, X., 2011. Estimating the relationship between urban forms and energy consumption: a case study in the Pearl River Delta, 2005-2008. Landsc. Urban Plan. 102 (1), 33–42. https://doi.org/10.1016/j.landurbplan.2011.03.007.

Chen, Y., Wong, N.H., 2006. Thermal benefits of city parks. Energy Build. 38 (2), 105–120. https://doi.org/10.1016/j.enbuild.2005.04.003.

Chun, B., Guldmann, J.M., 2014. Spatial statistical analysis and simulation of the urban heat island in high-density central cities. Landsc. Urban Plan. 125, 76–88. https://doi.org/10.1016/j.landurbplan.2014.01.016.

Conrad, O., Bechtel, B., Bock, M., Dietrich, H., Fischer, E., Gerlitz, L., Wehberg, J., Wichmann, V., and Böhner, J. 2015. System for Automated Geoscientific Analyses

(SAGA) v. 2.1.4. Geoscientific Model Development Discussions, 8(2), 2271–2312. https://doi.org/10.5194/gmdd-8–2271-2015.
Das, M., Das, A., 2020. Assessing the relationship between local climatic zones (LCZs) and land surface temperature (LST) – a case study of Sriniketan-Santiniketan Planning Area (SSPA), West Bengal, India. Urban Clim. 32, 100591 https://doi.org/10.1016/j.uclim.2020.100591.
De Castro, M., Gallardo, C., Jylha, K., Tuomenvirta, H., 2007. The use of a climate-type classification for assessing climate change effects in Europe from an ensemble of nine regional climate models. Clim. Change 81, 329–341. https://doi.org/10.1007/s10584-006-9224-1.
Dirksen, M., Ronda, R.J., Theeuwes, N.E., Pagani, G.A., 2019. Sky view factor calculations and its application in urban heat island studies. Urban Clim. 30, 100498 https://doi.org/10.1016/j.uclim.2019.100498.
Du, J., Xiang, X., Zhao, B., Zhou, H., 2020. Impact of urban expansion on land surface temperature in Fuzhou, China using Landsat imagery. Sustain. Cities Soc. 61, 102346 https://doi.org/10.1016/j.scs.2020.102346.
Dwivedi, A., Mohan, B.K., 2018. Impact of green roof on micro climate to reduce Urban Heat Island. Remote Sens. Appl.: Soc. Environ. 10, 56–69. https://doi.org/10.1016/j.rsase.2018.01.003.
Emmanuel, R., Krüger, E., 2012. Urban heat island and its impact on climate change resilience in a shrinking city: The case of Glasgow, UK. Build. Environ. 53, 137–149. https://doi.org/10.1016/j.buildenv.2012.01.020.
Fang, L., Tian, C., 2020. Construction land quotas as a tool for managing urban expansion. Landsc. Urban Plan. 195, 103727 https://doi.org/10.1016/j.landurbplan.2019.103727.
Feizizadeh, B., Blaschke, T., 2013. Examining Urban heat Island relations to land use and air pollution: Multiple endmember spectral mixture analysis for thermal remote sensing. IEEE J. Sel. Top. Appl. Earth Obs. Remote Sens. 6 (3), 1749–1756. https://doi.org/10.1109/JSTARS.2013.2263425.
Gago, E.J., Roldan, J., Pacheco, R., Ordóñez, J., 2013. The city and urban heat islands: a review of strategies to mitigate adverse effects. Renew. Sustain. Energy Rev. 25, 749–758. https://doi.org/10.1016/j.rser.2013.05.057.
Gaur, A., Eichenbaum, M.K., Simonovic, S.P., 2018. Analysis and modelling of surface Urban Heat Island in 20 Canadian cities under climate and land-cover change. J. Environ. Manag. 206, 145–157. https://doi.org/10.1016/j.jenvman.2017.10.002.
Guo, A., Yang, J., Xiao, X., Xia, J., Jin, C., Li, X., 2020. Influences of urban spatial form on urban heat island effects at the community level in China. Sustain. Cities Soc. 53, 101972 https://doi.org/10.1016/j.scs.2019.101972.
Hidalgo García, D., Arco Díaz, J., 2021. Modeling of the Urban Heat Island on local climatic zones of a city using Sentinel 3 images: urban determining factors. Urban Clim. 37. https://doi.org/10.1016/j.uclim.2021.100840.
Hidalgo, D., Arco, J., 2022. Remote Sensing Applications: Society and Environment Impacts of the COVID-19 confinement on air quality, the Land Surface Temperature and the urban heat island in eight cities of Andalusia (Spain). Remote Sens. Appl.: Soc. Environ. 25, 100667 https://doi.org/10.1016/j.rsase.2021.100667.
Hu, Y., Dai, Z., Guldmann, J.M., 2020. Modeling the impact of 2D/3D urban indicators on the urban heat island over different seasons: a boosted regression tree approach. J. Environ. Manag. 266 (11), 110424 https://doi.org/10.1016/j.jenvman.2020.110424.
Hua, L., Zhang, X., Nie, Q., Sun, F., Tang, L., 2020. The impacts of the expansion of urban impervious surfaces on urban heat islands in a coastal city in China. Sustainability 12 (2). https://doi.org/10.3390/su12020475.
Huryna, H., Cohen, Y., Karnieli, A., Panov, N., Kustas, W.P., Agam, N., 2019. Evaluation of TsHARP utility for thermal sharpening of Sentinel-3 satellite images using Sentinel-2 visual imagery. Remote Sens. 11 (19) https://doi.org/10.3390/rs11192304.
Karakuş, C.B., 2019. The Impact of Land Use/Land Cover (LULC) Changes on Land Surface Temperature in Sivas City Center and Its Surroundings and Assessment of Urban Heat Island. Asia-Pac. J. Atmos. Sci. 55 (4), 669–684. https://doi.org/10.1007/s13143-019-00109-w.
Khamchiangta, D., Dhakal, S., 2019. Physical and non-physical factors driving urban heat island: Case of Bangkok Metropolitan Administration, Thailand. J. Environ. Manag. 248, 109285 https://doi.org/10.1016/j.jenvman.2019.109285.
Kovats, R.S., Campbell-Lendrum, D., Matthies, F., 2005. Climate change and human health: Estimating avoidable deaths and disease. Risk Anal. 25 (6), 1409–1418. https://doi.org/10.1111/j.1539-6924.2005.00688.x.
Labra, R. 2014. Zero panel data guide. (Cátedra UA). file:///U:/Maguilera/Documentos Personales MAGUILERA/Master M3F/Trabajo Fin M3F/Revisión para paper/Referencias/Stata/16_Guia CERO para datos de panel_Un enfoque practico.pdf.
Lee, S.H., Lee, K.S., Jin, W.C., Song, H.K., 2009. Effect of an urban park on air temperature differences in a central business district area. Landsc. Ecol. Eng. 5 (2), 183–191. https://doi.org/10.1007/s11355-009-0067-6.
Li, J., Song, C., Cao, L., Zhu, F., Meng, X., Wu, J., 2011. Impacts of landscape structure on surface urban heat islands: a case study of Shanghai, China. Remote Sens. Environ. 115 (12), 3249–3263. https://doi.org/10.1016/j.rse.2011.07.008.
Lin, W., Yu, T., Chang, X., Wu, W., Zhang, Y., 2015. Calculating cooling extents of green parks using remote sensing: method and test. Landsc. Urban Plan. 134, 66–75. https://doi.org/10.1016/j.landurbplan.2014.10.012.
Lu, J., Li, C.D., Yang, Y.C., Zhang, X.H., Jin, M., 2012. Quantitative evaluation of urban park cool island factors in mountain city. J. Cent. South Univ. Technol. 19 (6), 1657–1662. https://doi.org/10.1007/s11771-012-1189-9.
Masoudi, M., Tan, P.Y., Fadaei, M., 2021. The effects of land use on spatial pattern of urban green spaces and their cooling ability. Urban Clim. 35. https://doi.org/10.1016/j.uclim.2020.100743.
Mukherjee, S., and Debnath, A. 2020. Correlation between Land Surface Temperature and Urban Heat Island with COVID-19 in New Delhi, India. 1–11. https://doi.org/10.21203/rs.3.rs-30416/v1.
Norton, T.A., Parker, S.L., Zacher, H., Ashkanasy, N.M., 2015. Employee green behavior: a theoretical framework, multilevel review, and future research agenda. Organ. Environ. 28 (1), 103–125. https://doi.org/10.1177/1086026615575773.
Olaya, V., Conrad, O., 2009. Geomorphometry in SAGA. Dev. Soil Sci. 33, 293–308. https://doi.org/10.1016/S0166-2481(08)00012-3.
Oliveira, S., Andrade, H., Vaz, T., 2011. The cooling effect of green spaces as a contribution to the mitigation of urban heat: a case study in Lisbon. Build. Environ. 46 (11), 2186–2194. https://doi.org/10.1016/j.buildenv.2011.04.034.
Qiu, G.Y., Zou, Z., Li, X., Li, H., Guo, Q., Yan, C., Tan, S., 2017. Experimental studies on the effects of green space and evapotranspiration on urban heat island in a subtropical megacity in China. Habitat Int. 68, 30–42. https://doi.org/10.1016/j.habitatint.2017.07.009.
Ray, D., Salvatore, M., Bhattacharyya, R., Wang, L., Du, J., Mohammed, S., Purkayastha, S., Halder, A., Rix, A., Barker, D., Kleinsasser, M., Zhou, Y., Bose, D., Song, P., Banerjee, M., 2020. Predictions, role of interventions and effects of a historic national lockdown in india's response to the COVID-19 pandemic: data science call to arms. Harv. Data Sci. Rev. 1. https://doi.org/10.1162/99608f92.60e08ed5.
Rongali, G., Keshari, A.K., Gosain, A.K., Khosa, R., 2018. A mono-window algorithm for land surface temperature estimation from landsat 8 thermal infrared sensor data: A case study of the beas river basin. India Pertanika J. Sci. Technol. 26, 829–40.
Saaroni, H., Amorim, J.H., Hiemstra, J.A., Pearlmutter, D., 2018. Urban Green Infrastructure as a tool for urban heat mitigation: Survey of research methodologies and findings across different climatic regions. Urban Clim. 24, 94–110. https://doi.org/10.1016/j.uclim.2018.02.001.
Safarrad, T., Ghadami, M., Dittmann, A., Pazhuhan, M., 2021. Tourism effect on the spatiotemporal pattern of land surface temperature (Lst): Babolsar and fereydonkenar cities (cases study in Iran. Land 10 (9). https://doi.org/10.3390/land10090945.
Santamouris, M., 2020. Recent progress on urban overheating and heat island research. Integrated assessment of the energy, environmental, vulnerability and health impact. Synerg. Glob. Clim. Change Energy Build. 207. https://doi.org/10.1016/j.enbuild.2019.109482.
Sarrat, C., Lemonsu, A., Masson, V., Guedalia, D., 2006. Impact of urban heat island on regional atmospheric pollution. Atmos. Environ. 40 (10), 1743–1758. https://doi.org/10.1016/j.atmosenv.2005.11.037.
Schneider, A., Friedl, M.A., Potere, D., 2010. Mapping global urban areas using MODIS 500-m data: new methods and datasets based on "urban ecoregions. Remote Sens. Environ. 114 (8), 1733–1746. https://doi.org/10.1016/j.rse.2010.03.003.
Seto, K.C., Kaufmann, R.K., 2003. Modeling the drivers of urban land use change in the Pearl River Delta, China: integrating remote sensing with socioeconomic data. Land Econ. 79 (1), 106–121. https://doi.org/10.2307/3147108.
Shafizadeh-Moghadam, H., Weng, Q., Liu, H., Valavi, R., 2020. Modeling the spatial variation of urban land surface temperature in relation to environmental and anthropogenic factors: a case study of Tehran, Iran. GIScience Remote Sens. 57 (4), 483–496. https://doi.org/10.1080/15481603.2020.1736857.
Sharma, A., Pandher, J.S., Prakash, G., 2022. Consumer confusion and decision postponement in the online tourism domain: the moderating role of self-efficacy. J. Hosp. Tour. Insights. https://doi.org/10.1108/JHTI-03-2O22-0096.
Shaver, G., Canadell, J., Chapin III, F., Gurevitch, J., Harte, J., Henry, G., Ineson, P., Jonasson, S., Melillo, J., Pitelka, Rustad, L., 2000. Global warming and terrestrial ecosystems: a conceptual framework for analysis. Bioscience 50 (10), 871–882. https://doi.org/10.1641/0006-3568(2000)050[0871:GWATEA]2.0.CO;2.
Solecki, W.D., Rosenzweig, C., Parshall, L., Pope, G., Clark, M., Cox, J., Wiencke, M., 2005. Mitigation of the heat island effect in urban New Jersey. Environ. Hazards 6 (1), 39–49. https://doi.org/10.1016/j.hazards.2004.12.002.
Song, J., Chen, W., Zhang, J., Huang, K., Hou, B., Prishchepov, A.V., 2020. Effects of building density on land surface temperature in China: spatial patterns and determinants. Landsc. Urban Plan. 198, 103794 https://doi.org/10.1016/j.landurbplan.2020.103794.
Spronken-Smith, T.R.O., 2010. The thermal regime of urban parks in two cities with different summer climates. Int. J. Remote Sens., June 2012, 37–41.
UN. 2018. 68% of the world population projected to live in urban areas by 2050, says UN. ⟨https://www.un.org/development/desa/en/news/population/2018-revision-of-world-urbanization-prospects.html⟩.
Upmanis, H., Eliasson, I., Lindqvist, S., 1998. The influence of green areas on nocturnal temperatures in a high latitude city (Goteborg, Sweden). Int. J. Climatol. 18 (6), 681–700. https://doi.org/10.1002/(SICI)1097-0088(199805)18:6<681::AID-JOC289>3.0.CO;2-L.
Van Hove, L.W.A., Jacobs, C.M.J., Heusinkveld, B.G., Elbers, J.A., Van Driel, B.L., Holtslag, A.A.M., 2015. Temporal and spatial variability of urban heat island and thermal comfort within the Rotterdam agglomeration. Build. Environ. 83, 91–103. https://doi.org/10.1016/j.buildenv.2014.08.029.
Wu, C., Li, J., Wang, C., Song, C., Chen, Y., Finka, M., La Rosa, D., 2019. Understanding the relationship between urban blue infrastructure and land surface temperature. Sci. Total Environ. 694. https://doi.org/10.1016/j.scitotenv.2019.133742.
Yoshida, A., Hisabayashi, T., Kashihara, K., Kinoshita, S., Hashida, S., 2015. Evaluation of effect of tree canopy on thermal environment, thermal sensation, and mental state. Urban Clim. 14, 240–250. https://doi.org/10.1016/j.uclim.2015.09.004.
Yu, X., Guo, X., Wu, Z., 2014. Land surface temperature retrieval from landsat 8 TIRS-comparison between radiative transfer equation-based method, split window

algorithm and single channel method. Remote Sens. 6 (10), 9829–9852. https://doi.org/10.3390/rs6109829.
Zakšek, K., Podobnikar, T., Oštir, K., 2005. Solar radiation modelling. Comput. Geosci. 31 (2), 233–240. https://doi.org/10.1016/j.cageo.2004.09.018.
Zhou, X., Wang, P., Tansey, K., Zhang, S., Li, H., Tian, H., 2020. Reconstruction of time series leaf area index for improving wheat yield estimates at field scales by fusion of Sentinel-2, -3 and MODIS imagery. Comput. Electron. Agric. 177 (17), 105692 https://doi.org/10.1016/j.compag.2020.105692.